The Astrophysical Journal, 780:127 (15pp), 2014 January 10 doi:10.1088/0004-637X/780/2/127

DISCOVERY OF THE THIRD TRANSIENT X-RAY BINARY IN THE GALACTIC GLOBULAR CLUSTER TERZAN 5

Arash Bahramian[1], Craig O. Heinke[1], Gregory R. Sivakoff[1], Diego Altamirano[2,3], Rudy Wijnands[2], Jeroen Homan[4], Manuel Linares[5,6], David Pooley[7,8], Nathalie Degenaar[9,10], and Jeanette C. Gladstone[1]
[1] Department of Physics, University of Alberta, CCIS 4-183, Edmonton, AB T6G 2E1, Canada; bahramia@ualberta.ca
[2] Astronomical Institute "Anton Pannekoek," University of Amsterdam, Science Park 904, 1098 XH Amsterdam, The Netherlands
[3] Physics & Astronomy, University of Southampton, Southampton, Hampshire SO17 1BJ, UK
[4] Kavli Institute for Astrophysics & Space Research, Massachusetts Institute of Technology, 70 Vassar Street, Cambridge, MA 02139, USA
[5] Instituto de Astrofísica de Canarias, c/Vía Láctea s/n, E-38205 La Laguna, Tenerife, Spain
[6] Universidad de La Laguna, Department Astrofísica, E-38206 La Laguna, Tenerife, Spain
[7] Department of Physics, Sam Houston State University, Huntsville, TX 77341, USA
[8] Eureka Scientific, Inc., 2452 Delmer Street, Suite 100, Oakland, CA, 94602, USA
[9] Department of Astronomy, University of Michigan, 500 Church Street, Ann Arbor, MI 48109, USA
Received 2013 August 21; accepted 2013 November 16; published 2013 December 17

ABSTRACT

We report and study the outburst of a new transient X-ray binary (XRB) in Terzan 5, the third detected in this globular cluster, Swift J174805.3-244637 or Terzan 5 X-3. We find clear spectral hardening in *Swift*/XRT data during the outburst rise to the hard state, thanks to our early coverage (starting at $L_X \sim 4 \times 10^{34}$ erg s^{-1}) of the outburst. This hardening appears to be due to the decline in relative strength of a soft thermal component from the surface of the neutron star (NS) during the rise. We identify a Type I X-ray burst in *Swift*/XRT data with a long (16 s) decay time, indicative of hydrogen burning on the surface of the NS. We use *Swift*/BAT, *MAXI*/GSC, *Chandra*/ACIS, and *Swift*/XRT data to study the spectral changes during the outburst, identifying a clear hard-to-soft state transition. We use a *Chandra*/ACIS observation during outburst to identify the transient's position. Seven archival *Chandra*/ACIS observations show evidence for variations in Terzan 5 X-3's nonthermal component but not the thermal component during quiescence. The inferred long-term time-averaged mass accretion rate, from the quiescent thermal luminosity, suggests that if this outburst is typical and only slow cooling processes are active in the NS core, such outbursts should recur every ∼10 yr.

Key words: binaries: close – globular clusters: individual (Terzan 5) – stars: neutron – X-rays: binaries – X-rays: bursts – X-rays: individual (Swift J174805.3-244637)

Online-only material: color figures

1. INTRODUCTION

Transient low-mass X-ray binaries (LMXBs) experience long periods (often years to tens of years) of quiescence. In quiescence matter flowing from the companion builds up in the accretion disk, punctuated by outbursts when the accretion disk crosses a pressure and temperature threshold, increases in viscosity, and dumps large quantities of matter onto the accreting compact object (e.g., see Lasota 2001, for a review). Their outbursts go through phases of varying X-ray spectra. These phases are generally interpreted as indicating the changing relative contributions of Comptonized optically thin emission versus blackbody-like emission from an accretion disk, as the accretion rate and geometry change (e.g., Remillard & McClintock 2006; Done et al. 2007, for reviews). These X-ray spectral states have been studied both for black hole LMXBs, and for neutron star (NS) LMXBs (e.g., Hasinger & van der Klis 1989; Gierliński & Done 2002; Gilfanov et al. 2003; Gladstone et al. 2007; Lin et al. 2007), which show an additional component from the NS surface.

The spectra of NS LMXBs in quiescence ($L_X \lesssim 10^{33}$ erg s^{-1}) include thermal radiation from the (usually hydrogen) NS atmosphere (blackbody-like; Zavlin et al. 1996; Rajagopal & Romani 1996), and often a harder nonthermal component, usually fit with a power-law (Campana et al. 1998). Several NS LMXBs have shown rapid, strong variability in quiescence indicative of accretion events, which can sometimes be clearly attributed to variation in both the thermal and power-law components (e.g., Rutledge et al. 2002; Campana et al. 2004; Cackett et al. 2010; Fridriksson et al. 2011). The thermal component can be produced either by re-radiation of stored heat from the cooling NS (Brown et al. 1998), or by low-level accretion (Zampieri et al. 1995; Deufel et al. 2001), which produce similar spectra (Zampieri et al. 1995).

Studies of the spectra of black hole LMXBs during their decline from the low/hard state into quiescence (as L_X falls below 10^{35} erg s^{-1}) have found clear softening (Corbel et al. 2006, 2008; Armas Padilla et al. 2013a; Plotkin et al. 2013). The softening of black hole LMXB spectra has been interpreted as a change in the origin of the X-ray emission, produced at low luminosities by either a radiatively inefficient hot flow (Esin et al. 1997; Gardner & Done 2012) or synchrotron emission from a jet (Yuan & Cui 2005; Pszota et al. 2008). A similar softening in the spectrum from the accretion flow occurs in NS systems at similar luminosities, where emission from the NS surface can play a role (Armas Padilla et al. 2011; Degenaar et al. 2013b; M. Linares et al. 2013).

Thermonuclear X-ray bursts burn accumulated hydrogen and/or helium on the NS surface, producing blackbody-like emission with a rapid rise, cooling over timescales of seconds to minutes (Lewin et al. 1993; Galloway et al. 2008). X-ray bursts occurring in hydrogen-poor environments (either due to

[10] Hubble Fellow.

no hydrogen being present in the accreted material, or hydrogen being stably burned during accretion) show different properties from those in hydrogen-rich environments. The ratio of energy released by fusion in a burst to energy released during accretion is lower for helium bursts compared to hydrogen bursts due to the lower energy available from fusion.

Helium bursts generally have faster rise and decline times, since hydrogen burning involves the CNO cycle and thus is limited by the speed of β-decays (Fujimoto et al. 1981). Pure He bursts can be ignited in NSs that accrete hydrogen at low mass accretion rates (e.g., Peng et al. 2007), but NSs known to be accreting hydrogen-poor material (ultracompact systems with white dwarf donors) never show evidence of hydrogen-rich bursts (Galloway et al. 2008). Some bursts from ultracompact systems are relatively long, but these "giant" (or "intermediate-duration") bursts exhibit dramatic photospheric radius expansion, thought to be produced by a thick layer of accumulated He, which can accumulate only at low ($L_X < 0.01 L_{\rm Edd}$) accretion rates (in't Zand et al. 2005).

Globular clusters are highly efficient at producing X-ray binaries through dynamical interactions, such as the exchange of (heavy) NSs into pre-existing binary stars, replacing the lower-mass star in the binary. Of perhaps 200 galactic LMXBs known to have reached $L_X \sim 10^{36}$ erg s^{-1}, 18 (including Terzan 5 X-3) are located in globular clusters, a factor of ~100 overabundance per unit stellar mass compared to the galactic disk. LMXBs are concentrated in the densest, most massive globular clusters, which have the highest predicted rates of stellar interactions (e.g., Verbunt & Hut 1987; Heinke et al. 2003c). Studying the number and types of LMXBs in different globular clusters can help us understand the dynamical processes that produce LMXBs in clusters. For example, identifying multiple LMXBs in one cluster has implications for interpreting observations of X-ray emission from extragalactic globular clusters (such as their luminosity functions), where multiple LMXBs cannot be resolved (e.g., Sivakoff et al. 2007). Before Terzan 5 X-3, no more than two bright LMXBs had been identified in any one globular cluster (White & Angelini 2001; Heinke et al. 2010; Pooley et al. 2010).

Terzan 5 is a dense and massive globular cluster close to the center of our Galaxy ($d = 5.9 \pm 0.5$ kpc; Valenti et al. 2007), showing evidence of two separate stellar populations of different iron abundances, ages and helium content (Ferraro et al. 2009; D'Antona et al. 2010). Calculations of its stellar encounter rate suggest it may produce more X-ray binaries than any other Galactic globular cluster (Verbunt & Hut 1987; Lanzoni et al. 2010; Bahramian et al. 2013). This status is supported by the largest population of known millisecond radio pulsars in any globular cluster, which are thought to be the descendants of LMXBs (Ransom et al. 2005; Hessels et al. 2006). Terzan 5 also hosts more than 50 known X-ray sources (Heinke et al. 2006b), including a dozen likely quiescent LMXBs (again the most numerous in any cluster).

Outburst of transient LMXBs have frequently been observed from Terzan 5 (Makishima et al. 1981; Warwick et al. 1988; Verbunt et al. 1995). *Chandra* observed one such outburst in 2000 (Heinke et al. 2003a), pinning down the location of an LMXB called EXO 1745-248,[11] which was shown to have an unusually hard spectrum in quiescence during later *Chandra* observations (Wijnands et al. 2005; Degenaar & Wijnands 2012). Another Terzan 5 outburst was identified in 2002 in *RXTE* All-Sky Monitor data (Wijnands et al. 2002a), but no imaging observations were taken. In 2010 an outburst was seen from an 11 Hz pulsar, IGR J17480-2446 (Terzan 5 X-2, Bordas et al. 2010; Strohmayer & Markwardt 2010), leading to a variety of detailed studies of the orbit and spin period, bursts, spectrum, burst oscillations, and evolution (e.g., Papitto et al. 2011; Chakraborty et al. 2011; Miller et al. 2011; Motta et al. 2011; Cavecchi et al. 2011; Linares et al. 2011, 2012; Patruno et al. 2012; Papitto et al. 2012; Altamirano et al. 2012a). A *Chandra* observation identifying the outbursting source (Pooley et al. 2010) allowed follow-up observations to track the crustal cooling of the NS (Degenaar et al. 2011; Degenaar & Wijnands 2011; Degenaar et al. 2013a), while the even more precise moon occultation position (Riggio et al. 2012) permitted identification of the near-IR counterpart (Testa et al. 2012). Another Terzan 5 outburst, in 2011, was identified as EXO 1745-248 through a *Chandra* observation (Pooley et al. 2011a), and showed a superburst (a very long and energetic X-ray burst, thought to be powered by the burning of a thick layer of carbon) at the beginning of the outburst (Serino et al. 2012; Altamirano et al. 2012b)

In this paper we identify and study the outburst of the third transient X-ray binary in the globular cluster Terzan 5, Swift J174805.3-244637 (henceforth Terzan 5 X-3). We detected this transient using *Swift*/XRT (Wijnands et al. 2012), and identified spectral hardening in the rise of the outburst (Heinke et al. 2012), a Type I X-ray burst (Altamirano et al. 2012c), and the quiescent X-ray counterpart in *Chandra* images (Homan & Pooley 2012). In Section 2 we present the X-ray data used and describe our data extraction. In Section 3 we derive the position of Terzan 5 X-3 by comparing observations before and during the outburst, analyze the spectral variation of the persistent emission throughout the outburst, study the properties of the thermonuclear burst, and analyze its quiescent X-ray spectrum. Finally, we discuss our results in Section 4.

2. DATA EXTRACTION

2.1. *Swift*/XRT

We monitored Terzan 5 up to a few times per week for part of 2012 with the *Swift*/XRT, covering the 0.3–10 keV energy range (Burrows et al. 2005), as part of our monitoring campaigns of globular cluster X-ray transients (see Altamirano et al. 2012b; D. Altamirano et al. 2013, in preparation). This monitoring enabled us to observe the rising outburst of a new transient (and the 3rd known transient LMXB in this cluster) first detected on 2012 July 6 (Wijnands et al. 2012).

We used *Swift*/XRT's photon counting (PC) mode, which produces two-dimensional images, and windowed timing (WT) mode for which CCD data is collapsed into a one-dimensional image for fast readout. PC mode data should be checked for pile-up when the count rate exceeds 0.5 count s^{-1}. Pile-up is the recording of multiple photons as a single event, leading in the worst case to rejection of all events from the center of the point-spread function, or PSF. Our *Swift*/XRT observations include 22 observations during the outburst, with 8 observations in WT and the rest in PC mode (Table 1).

We used HEASOFT 6.12 and FTOOLS[12] (Blackburn 1995) to reduce and analyze the data. We reprocessed the data with the FTOOLS *xrtpipeline* and manually extracted data for spectral analysis. We investigated every observation for pile-up,

[11] Note that the true identity of the transient seen by EXOSAT in the 1980s (leading to the EXO name) is not known.

[12] http://heasarc.gsfc.nasa.gov/ftools/

Table 1
List of *Swift*/XRT Observations (Top) and *Chandra*/ACIS Observations (Bottom) of Terzan 5 Used

Obs. ID	Date	MJD	Exposure	Avg. Count Rate (count s^{-1})	Notes
			Swift/XRT observations		
32148002	2012 Feb 9	55966.9	985 s	1.75×10^{-2}	PCmode; quiescent
91445001	2012 Jun 11	56089.8	913 s	2.67×10^{-2}	PCmode; quiescent
91445002	2012 Jun 16	56094.5	1028 s	1.48×10^{-2}	PCmode; quiescent
91445003	2012 Jun 21	56099.0	1033 s	1.66×10^{-2}	PCmode; quiescent
91445004	2012 Jun 26	56104.8	1050 s	9.68×10^{-3}	PCmode; quiescent
91445005	2012 Jun 30	56108.6	935 s	1.40×10^{-2}	PCmode; quiescent
91445006	2012 Jul 6	56114.8	1197 s	7.65×10^{-2}	PCmode; First detection of rise; (1)
32148003	2012 Jul 7	56115.8	987 s	0.154	PCmode; (2)
32148004	2012 Jul 8	56117.0	987 s	0.245	PCmode; (2)
32148005	2012 Jul 10	56118.1	781 s	1.26	PCmode; Piled up; (2)
32148006	2012 Jul 12	56120.7	978 s	3.19	PCmode; Piled up; Hard/soft transition
526511000	2012 Jul 13	56121.7	251 s	11.4	WTmode
91445008	2012 Jul 16	56124.3	253 s	14.2	WTmode
526892000	2012 Jul 16	56124.9	596 s	14.9	WTmode
32148007	2012 Jul 17	56125.9	960 s	20.4(16.3)[a]	WTmode; Type I X-ray burst; (3)
91445009	2012 Jul 21	56129.1	1173 s	71.8	WTmode
91445010	2012 Jul 26	56134.1	612 s	23.5	PCmode; Piled up
91445011	2012 Aug 1	56140.1	985 s	52.1	WT mode
91445012	2012 Aug 5	56144.8	1057 s	24.1	WTmode; Return to hard state?
91445013	2012 Aug 10	56149.4	1031 s	4.15	WTmode
32148008	2012 Aug 11	56150.1	1488 s	3.16	PCmode; Piled up
32148011	2012 Aug 13	56152.2	1480 s	2.47	PCmode; Piled up
530808000	2012 Aug 13	56152.4	774 s	2.97	PCmode; Piled up
32148010	2012 Aug 14	56153.2	1494 s	2.51	PCmode; Piled up
91445014	2012 Aug 15	56154.3	1060 s	2.17	PCmode; Piled up
32148012	2012 Aug 19	56158.3	2153 s	1.78	PCmode; Piled up
91445015	2012 Aug 20	56159.1	1006 s	2.14	PCmode; Piled up
91445016	2012 Aug 24	56163.2	1131 s	1.05	PCmode
32148013	2012 Aug 30	56169.3	2075 s	2.95×10^{-2}	PCmode; quiescent
32148014	2012 Sep 13	56177.6	1953 s	2.02×10^{-2}	PCmode; quiescent
32148015	2012 Sep 20	56184.6	1976 s	1.98×10^{-2}	PCmode; quiescent
			Chandra/ACIS observations		
3798	2003 Jul 13	52833.6	39.34 ks	9.91×10^{-3}	quiescent; (4, 5)
10059	2009 Jul 15	55027.7	36.26 ks	7.42×10^{-3}	quiescent; (6, 7)
13225	2011 Feb 17	55609.3	29.67 ks	5.56×10^{-3}	quiescent; (6, 7)
13252	2011 Apr 29	55680.7	39.54 ks	6.78×10^{-3}	quiescent; (7, 8)
13705	2011 Sep 5	55809.7	13.87 ks	5.69×10^{-3}	quiescent; (9)
14339	2011 Sep 8	55812.1	34.06 ks	6.08×10^{-3}	quiescent; (9)
13706	2012 May 13	56060.7	46.46 ks	7.58×10^{-3}	quiescent; (9)
13708	2012 Jul 30	56138.4	9.84 ks	6.60	Terzan 5 X-3 outburst; Piled up; (10, 11)

Notes. [a] The second count rate is calculated excluding the X-ray burst interval. Reported count rates are not corrected for pile up. MJDs are reported for start of each observation.

References. (1) Wijnands et al. 2012; (2) Heinke et al. 2012; (3) Altamirano et al. 2012c; (4) Wijnands et al. 2005; (5) Heinke et al. 2006b; (6) Degenaar et al. 2011; (7) Degenaar & Wijnands 2011; (8) Degenaar & Wijnands 2012; (9) Degenaar et al. 2013a; (10) Homan & Pooley 2012; (11) this work.

following the *Swift*/XRT pile-up thread,[13] and extracted data from an annulus around the source in PC mode observations that suffered from pile-up. We subtracted background from a circular region in the vicinity of the source in all PC observations. The extraction region for WT data was chosen to be a box around the event array (background subtraction was unnecessary for these count rates), as discussed in the *Swift*/XRT data reduction guide.[14] We extracted spectra in the 0.5–10 keV bandpass using FTOOLS *xselect*, and created ancillary response function (ARF) files for each observations using FTOOLS *xrtmkarf*. We performed spectral analysis using XSPEC 12.7.1 (Arnaud 1996).

For heavily absorbed sources, WT data show low energy spectral residuals, which look like a "bump" in the spectrum, and cause spectral uncertainties in the $\lesssim$1.0 keV region.[15] We compared *Swift*/XRT WT mode data to *Chandra* data (Section 2.2) taken within a few days, fitting them with the same model to find the energy range in which discrepancies appear. Based on this comparison, we ignored data below 1.4 keV in all WT observations during the outburst.

2.2. *Chandra*/ACIS

We observed Terzan 5 X-3 during outburst with *Chandra*/ACIS in full-frame and FAINT telemetry mode with no grating (Obs. ID: 13708, PI: Pooley). We also used *Chandra* archival

[13] http://www.swift.ac.uk/analysis/xrt/pileup.php
[14] http://heasarc.nasa.gov/docs/swift/analysis
[15] http://www.swift.ac.uk/analysis/xrt/digest_cal.php

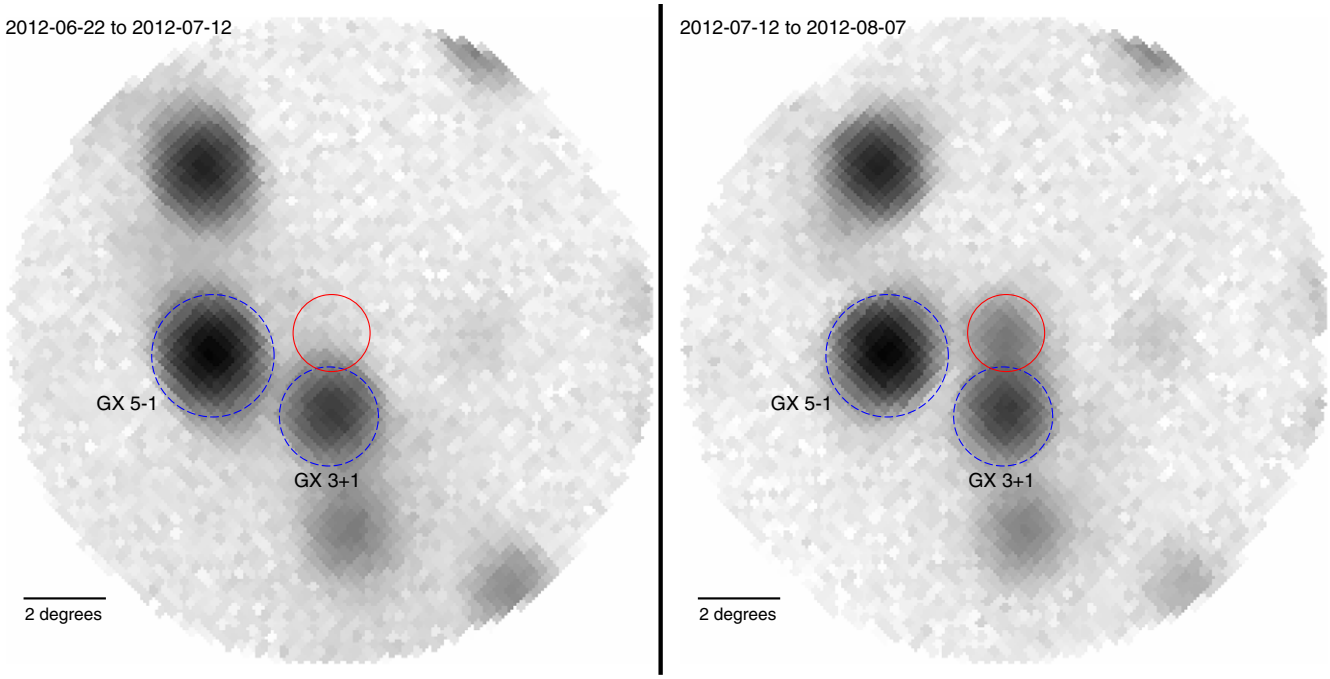

Figure 1. *MAXI*/GSC 2–20 keV images of the sky around Terzan 5 (the red circle). Left: before Terzan 5 X-3 outburst. Right: during the outburst. *MAXI*/GSC data for Terzan 5 may suffer contamination from the nearby sources GX 5-1 and GX 3+1 (blue dashed circles).
(A color version of this figure is available in the online journal.)

data for our analysis of this source, details of which can be found in Table 1. All archival observations were taken in FAINT telemetry mode with the ACIS-S3 CCD at the focus. We analyze *Chandra*/ACIS data in the 0.5–10 keV energy range.

Data was reprocessed using CIAO 4.4 (Fruscione et al. 2006), with CALDB 4.4.8, following the standard CIAO science threads.[16] We used observations during which all sources in the globular cluster were in quiescence. We reprocessed the data, corrected the relative astrometry and ran CIAO *reproject_events*, and then stacked the event files together using CIAO *dmmerge*.

Spectra were then extracted from both the archival and new data using CIAO task *dmextract*. Terzan 5 X-3 was heavily piled up in the new observation (in outburst), and so we extracted a spectrum from the readout streak. Finally, we combined all archival (quiescent data) using FTOOLS *addspec*.[17] Combining the quiescent data resulted in 240 ks of exposure time.

2.3. MAXI/GSC

The *MAXI* all sky X-ray monitor's (Matsuoka et al. 2009) *GSC* detector data covers the 2–20 keV energy range, and one-day averaged light curves are publicly provided in four bands: 2–4 keV, 4–10 keV, 10–20 keV and 2–20 keV (Mihara et al. 2011). We noticed two problems with *MAXI*/GSC light curves. Due to the low spatial resolution of *MAXI*/GSC and bright sources in the crowded field of Terzan 5, there is the possibility of background contamination from nearby sources like GX 3+1 and GX 5-1 (Figure 1). Since these two sources showed stable X-ray brightness with no obvious variations in the *MAXI*/GSC data during Terzan 5 X-3 outburst, the background contamination may lead to a constant enhanced background.

We also noticed that *MAXI*/GSC light curves show periodic behavior with a period of ≈35 days for various well-known stable X-ray sources (e.g., the Crab nebula). This is caused by calibration issues regarding the 70-day precession of the International Space Station's orbit (*MAXI* team 2013, private communication). This problem principally affects the 2–4 keV data, with less effect on the 4–10 and 10–20 keV light curves. Thus we ignored the 2–4 keV light curves for this research. We also ignored *MAXI*/GSC 10–20 keV band light curves, due to the low statistical significance of Terzan 5 X-3's detection there. We decontaminated the *MAXI*/GSC 4–10 keV light curve assuming a constant background count rate of 0.023, calculated based on a weighted average of the count rates before the outburst for a period of ∼120 days, with the addition of a systematic error based on the rms variations in the light curve before the outburst. We used the corrected values of the statistical uncertainties in *MAXI*/GSC data, as the *MAXI* team announced an erratum in the reported statistical uncertainties on 2013 April 26 (*MAXI* team 2013, private communication) noting that the corrected uncertainties are a factor of two larger than previously reported.

2.4. Swift/BAT

The *Swift*/BAT telescope data covers 15–150 keV energy range (Barthelmy et al. 2005). We used daily light curves from the *Swift*/BAT transient monitor results provided by the *Swift*/BAT team (Krimm et al. 2013). Data points on these daily light curves are from *Swift*/BAT survey data and are represented in a single band (15–50 keV). These points are the weighted average of all observations performed each day. The Swift/BAT has better angular resolution (20 vs.1 degree FWHM for Swift/BAT versus MAXI/GSC). Such an improvement in the angular resolution limits the chances of contamination occurring. Although we cannot rule out some contamination, it seems reasonable that it does not pose a serious problem. As such, it is not surprising that we do not see evidence of contamination of the Swift/BAT data by nearby sources as is identifiable in the MAXI data.

[16] http://cxc.harvard.edu/ciao/threads/index.html
[17] We found the results from CIAO's *combine_spectra* and FTOOLS's *addspec* completely identical.

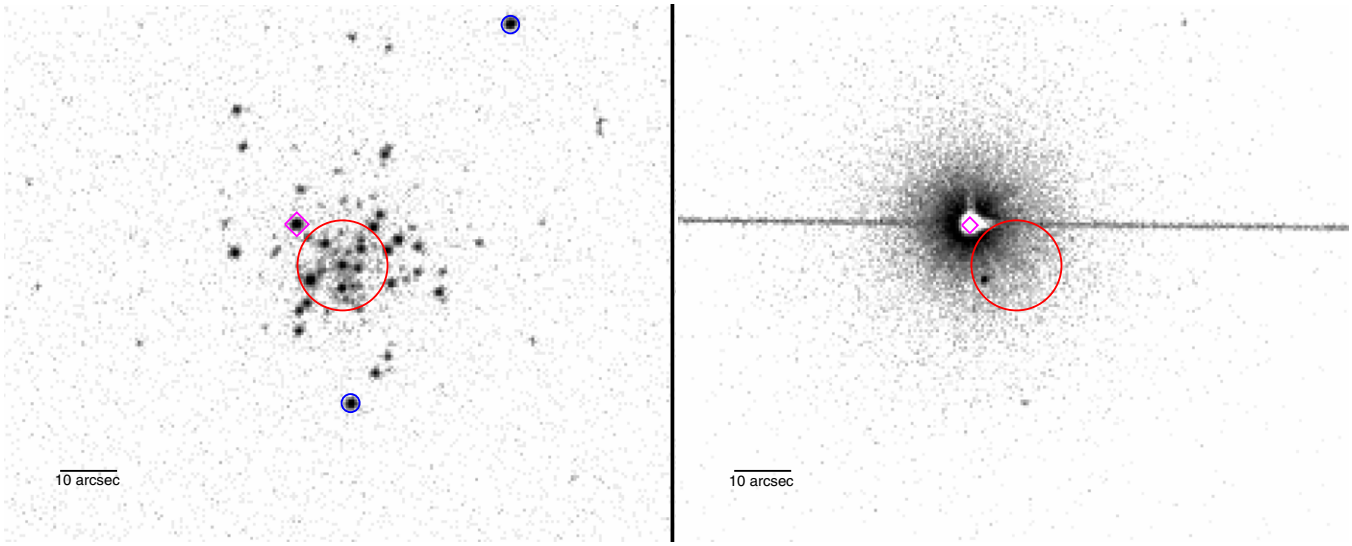

Figure 2. *Chandra*/ACIS observations of Terzan 5. Left: stacked image of observations during quiescence (bottom of Table 1) of all sources; total exposure ≈240 ks. Right: outburst of Terzan 5 X-3 (Obs. ID 13708 with exposure ≈10 ks). The red circles and magenta diamond represent the core of Terzan 5 (Harris 1996) and the position of Terzan 5 X-3, respectively (before astrometric corrections to the outburst image). Blue circles identify additional sources (CXOGLB J174804.7-244709 and CXOGLB J174802.6-244602) used for constraining the hydrogen column density of Terzan 5 (Section 3.3.1).

(A color version of this figure is available in the online journal.)

3. ANALYSIS AND RESULTS

3.1. Position

We accurately and precisely located the position of Terzan 5 X-3, using the *Chandra*/ACIS data. We compared the *Chandra*/ACIS observation taken during the outburst and a stacked image of 7 *Chandra*/ACIS observations taken when all Terzan 5 sources were in quiescence (Section 2.2, Table 1). We corrected the astrometry in the outburst observation by comparing the positions (using the CIAO *wavdetect* tool) of three other sources in this observation with their astrometrically corrected positions as reported in Heinke et al. (2006b). Using a weighted average of the required shifts (+0.″23 for R.A. and +0.″04 for Decl.), we find the position of Terzan 5 X-3 to be R.A. = 17:48:05.ˢ41 ± 0.ˢ02 and Decl. = −24:46:38.″0 ± 0.″2, in agreement (2σ) with the published position of the X-ray source CXOGLB J174805.4-244637 (Heinke et al. 2006b), at R.A. = 17:48:05.ˢ413 ± 0.ˢ001 and Decl. = −24:46:37.″67 ± 0.″02 (Figure 2).

3.2. Phases of the Outburst

We used *MAXI*/GSC and *Swift*/BAT hard X-ray transient monitor light curves to study the evolution of Terzan 5 X-3's outburst in the soft X-ray (4–10 keV, *MAXI*/GSC) and hard X-ray (15–50 keV, *Swift*/BAT) bands. We converted count rates into equivalent fluxes from the Crab Nebula to make these light curves suitable for comparison. For this purpose, we used conversion coefficients given for each instrument[18]: for the *Swift*/BAT hard X-ray transient monitor 1 Crab = 0.22 count cm^{-2} s^{-1} and for the *MAXI*/GSC 4–10 keV band 1 Crab = 1.24 count cm^{-2} s^{-1}. We plot the light curves for Terzan 5 X-3's outburst as seen by both *MAXI*/GSC and *Swift*/BAT, and their ratio, in Figure 3.

We distinguish four phases of Terzan 5 X-3's outburst. (a) Rise: the hard X-ray brightness of the source increases, the source eventually becoming significantly detected in the soft X-ray as well. (b) Hard state: hard X-ray brightness reaches its peak. (c) Soft state: soft X-ray brightness peaks while hard X-ray brightness drops. (d) Decline: the source briefly gets brighter in the hard X-ray again before turning off. Unfortunately there is insufficient data from the MAXI /GSC during the decline of the outburst. Therefore, we are unable to confirm that Terzan 5 X-3 returns to the hard state during its decline.

We used the soft X-ray (*MAXI*/GSC 4–10 keV, S) and hard X-ray (*Swift*/BAT 15–50 keV, H) light curves, to create a color–luminosity diagram (as an analogy to a hardness–intensity diagram, Fender et al. 2004) for the outburst (Figure 4). We defined our color to be $(H - S)/(H + S)$, and defined luminosity as $(H + S)$, converting count rates to luminosities in each band before their summation or subtraction. We converted count rates to luminosities with the assumption of a 5.9 kpc distance and power-law spectra, using power-law index values inferred from *Swift*/XRT data spectral fitting (Section 3.3.2). We extrapolated the *MAXI*/GSC 4–10 keV band flux to 0.1–12 keV and the *Swift*/BAT 15–50 keV band flux to 12–50 keV, and calculated luminosities in the 0.1–50 keV band. We cannot measure the spectral index above 10 keV, but since in the hard state the spectra are typically reasonably described by a power-law up to 50 keV, and in the soft state the flux above 12 keV is a minor contribution to the total, this is unlikely to have a large effect. In the 0.5–10 keV band, the source was bright for approximately 20 days, reaching a maximum luminosity of 7×10^{37} erg s^{-1} and an average luminosity of 3×10^{37} erg s^{-1} in this time interval. The evolution of the outburst and phases mentioned above can be clearly seen in this color–luminosity diagram (Figure 4). Spectral evolution during the outburst, including at fainter fluxes but with a more limited bandpass, can also be seen in *Swift*/XRT observations (Section 3.3.2).

3.3. Spectral Analysis

3.3.1. Hydrogen Column Density of Terzan 5

The first step in our spectral analysis is constraining hydrogen column density $N_{\rm H}$, which we check by spectral analysis of multiple sources in the cluster. Since the sources are located

[18] *MAXI*- http://maxi.riken.jp/top/index.php?cid=000000000036 *Swift*/BAT-http://swift.gsfc.nasa.gov/docs/swift/results/transients

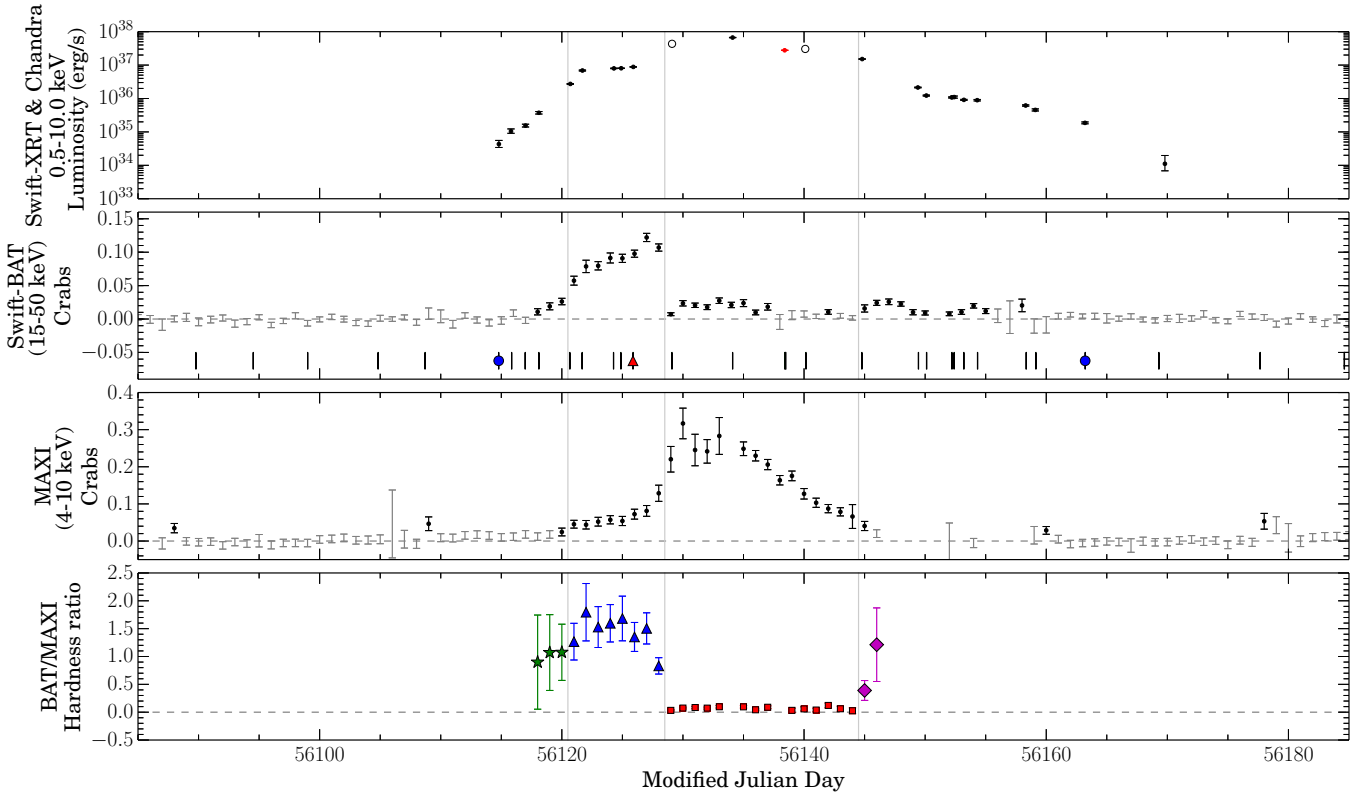

Figure 3. Evolution of Terzan 5 X-3 outburst. From the top, first panel: luminosities from spectral fitting of *Swift*/XRT and *Chandra*/ACIS pointed observations (Section 3.3.2). Empty circles represent observations where these fits were poor ($\chi^2_\nu > 2$). The red data point represents *Chandra*/ACIS observation. Second panel: *Swift*/BAT light curve in the 15–50 keV band. Third panel: *MAXI*/GSC background-subtracted light curve in the 4–10 keV band. Fourth panel: hardness ratio (H/S after conversion to Crab units) of the two light curves (*Swift*/BAT/*MAXI*/GSC). Black data points in the upper two panels represent significant detections ($>2\sigma$) in each band, while gray bars show times when Terzan 5 X-3 was not significantly detected. Vertical lines at the bottom of the first panel represent times of pointed *Swift*/XRT and *Chandra*/ACIS observations. The first and last detections of the outburst in *Swift*/XRT data are represented by blue circles. The red triangle identifies the time of the detected thermonuclear burst (Section 3.3.3). Colors and shapes in the bottom panel indicate the different phases of outburst: (a) green stars, rise, (b) blue triangles, hard state, (c) red squares, soft state, (d) magenta diamonds, decline. Both *Swift*/BAT and *MAXI*/GSC light curves are in Crab units, and error bars are 1σ uncertainties. Vertical lines in panels show approximate boundary of introduced phases. Note that in the fourth panel symbol size is larger than the error bars in the soft state. All daily averages are plotted at the beginning of each day.

(A color version of this figure is available in the online journal.)

within $1'$ of each other, we expect little variation in $N_{\rm H}$ along the different sightlines. Except for LMXBs observed at high inclination, generally the measured $N_{\rm H}$ throughout an outburst appears to be stable (Miller et al. 2009), so we assume that Terzan 5 X-3's $N_{\rm H}$ remains constant. We used *Chandra*/ACIS observations of Terzan 5 taken when all sources were quiescent (Table 1). We extracted spectra of three of the brighter faint sources in Terzan 5 (Terzan 5 X-3, CXOGLB J174804.7-244709 and CXOGLB J174802.6-244602; Heinke et al. 2006b; Figure 2) from each observation using CIAO *dmextract* and combined the extracted spectra for each source. We fit these combined spectra, along with the *Chandra* spectrum of Terzan 5 X-3 during the outburst, simultaneously. We used appropriate models based on previous studies of each faint source (Heinke et al. 2006b), confirmed as acceptable fits. For Terzan 5 X-3 during quiescence, and for CXOGLB J 174804.7-244709, we used a NS atmosphere (NSATMOS; Heinke et al. 2006a) plus a power-law (PEGPWRLW). For CXOGLB J 174802.6-244602 we used a power-law. Finally, for Terzan 5 X-3 during outburst, we used a disk model (DISKBB) plus a thermal Comptonization model (COMPTT; Titarchuk 1994). We fit all these spectra simultaneously with a single value of $N_{\rm H}$, using the PHABS model in XSPEC, with Anders & Grevesse (1989) abundances, finding $N_{\rm H} = 1.74^{+0.06}_{-0.08} \times 10^{22}$ cm^{-2}. Individual spectral fits gave consistent results, with differences below the 10% level. This value is consistent with the measurements in Heinke et al. (2003a), Wijnands et al. (2005), Heinke et al. (2006b), and Degenaar et al. (2011), though not with the lower value of Miller et al. (2011),[19] and is consistent with the $E(B-V)$ estimates in Valenti et al. (2007) and Massari et al. (2012), using the Güver & Özel (2009) relation to $N_{\rm H}$. We note that Miller et al. (2011) fit a simple blackbody plus power-law to the outburst spectrum of IGR J17480-2446 (Terzan 5-X2), which may lead to systematic differences compared to more complex outburst spectral models. We used our best-fit $N_{\rm H}$ value in the PHABS model, using default abundances, for the rest of the spectral analysis throughout this paper.

For comparison, we also used the same procedure for constraining $N_{\rm H}$ using the TBABS model (instead of PHABS), with Wilms et al. (2000) abundances, finding an increase in $N_{\rm H}$ to $2.6 \pm 0.1 \times 10^{22}$ cm^{-2}. The remaining parameters agreed within the errors with the results using our default absorption model, indicating that for our level of analysis only internal consistency is required in the choice of absorption model.

3.3.2. Outburst

The spatial resolution of *Swift*/XRT is such that we must account for possible contamination due to emission form other XRBs in the cluster. To assess these levels, we fit the spectra

[19] Miller et al. (2011) report $N_{\rm H} = (1.17 \pm 0.04) \times 10^{22}$ cm^{-2}, though they do not report the abundance scale they use.

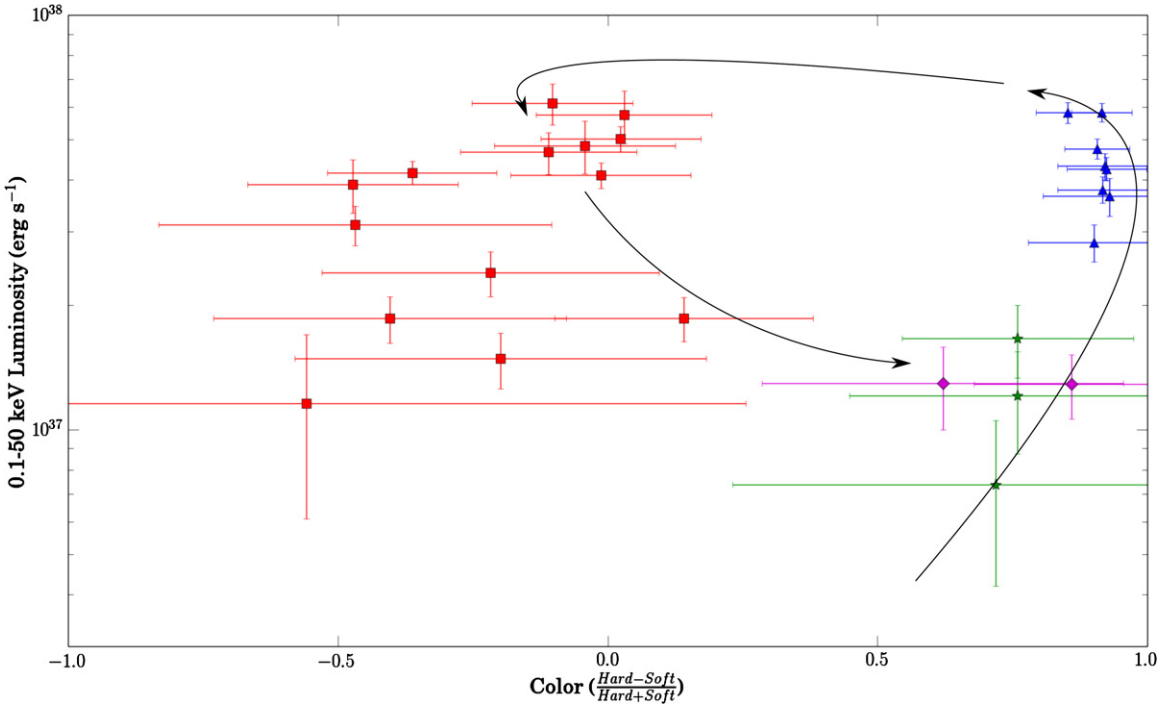

Figure 4. Color–luminosity diagram of Terzan 5 X-3 outburst, using the soft X-ray (*MAXI*/GSC 4–10 keV, *S*) and hard X-ray (*Swift*/BAT 15–50 keV, *H*) light curves, each in erg s^{-1} (Section 3.2). Color is $(H - S)/(H + S)$, while luminosity is $(H + S)$. Colors and shapes of points indicate the phases of outburst (as in Figure 3): (a) green stars, rise, (b) blue triangles, hard state, (c) red squares, soft state, (d) magenta diamonds, decline. Arrows represent the chronological order of data points. Error bars indicate 1σ uncertainties.

(A color version of this figure is available in the online journal.)

of pre-outburst observations (using the same extraction region as for the outburst spectra), finding a background level of $L_X \sim 10^{34}$ erg s^{-1}. We used 6 *Swift*/XRT observations taken before the outburst to estimate the combined spectrum from the other cluster sources. Due to the low number of counts per observation, we combined their spectra. We fit the resulting pre-outburst spectrum with an absorbed power-law model (Table 2) with $N_{\rm H}$ fixed to 1.74×10^{22} cm^{-2}, based on the results in Section 3.3.1.

For our initial spectral analysis, we used an absorbed power-law model to fit Terzan 5 X-3's spectrum, including a second power-law component with values fixed to the pre-outburst results to model the background (Table 2, Figure 5). A simple power-law model provided a good fit to most of the spectra (Table 2), while physically motivated complex spectral models could not be well-constrained for the high-quality bright outburst spectra (see below), so we focus on the results from power-law fits. This spectral analysis shows a significant drop of photon index from 2.6 ± 0.7 to 1.4 ± 0.1 during the outburst rise (Figure 5), showing a clear hardening of the spectrum during the rise from quiescence. During the hard state, the photon index shows no significant variations and is $\approx$1.4. After the phase transition to the soft state, the photon index softens to $\approx$1.9, with significant variations and several poor fits.

Several spectral models have been suggested in the literature to model the detailed spectra of transient NS LMXBs in outburst, see e.g., Lin et al. (2007). These models usually contain a soft component for the radiation from the disk and/or boundary layer(i.e., a multi-color black body) and a hard component for the radiation from the hot corona around the accreting object (i.e., Comptonized radiation). We attempted to perform analyses of Terzan 5 X-3's outburst spectra using a variety of complex models with multiple components (e.g., DISKBB + COMPTT, BBODY+COMPTT, BBODY+BKNPOW). We could not obtain strong constraints on the spectral parameters due to the limited energy band available and limited statistical quality of the XRT data. The *Swift*/XRT WT spectra suffered particularly from calibration issues below $\sim$1 keV (Section 2.1). The *Swift*/BAT survey mode hard (>15 keV) X-ray spectra had a low signal to noise ratio, which prohibited spectral analysis. We defer further detailed spectral fitting, e.g., to clearly distinguish thermal versus nonthermal components, to future work.

3.3.3. Thermonuclear Burst

During *Swift*/XRT ObsID 32148007, which started at 20:54:00 UT on 2012 July 17, we detected an eightfold count rate increase over $\sim$3 s, starting at $\approx$21:06:40, followed by a slower decline over $\sim$1 minute (Figure 6, bottom panel), suggestive of a thermonuclear burst (Altamirano et al. 2012c). Using FTOOLS *xselect*, we divided the data from this observation into time intervals of 4 s each. We extracted spectra from each time interval using FTOOLS *xselect* and analyzed the spectra.

During this thermonuclear burst, the count rate reached $\approx$160 count s^{-1}. There is a possibility of pileup in *Swift*/XRT observations in windowed timing mode when the count rate exceeds 100 count s^{-1} (Romano et al. 2006). Following the *Swift*/XRT pile-up thread for WT data, we extracted spectra while excluding increasingly large fractions of the central PSF. Doing this, we found that the fitted photon index did not change, and thus we found no significant signs of pileup in this observation during the burst.

We fit an absorbed power-law to the spectrum extracted from a pre-burst interval, and considered this fit as a fixed component of the spectral model for time intervals during the burst (cf., Worpel et al. 2013; our statistics are insufficient to determine whether this assumption is correct, and moderate changes should

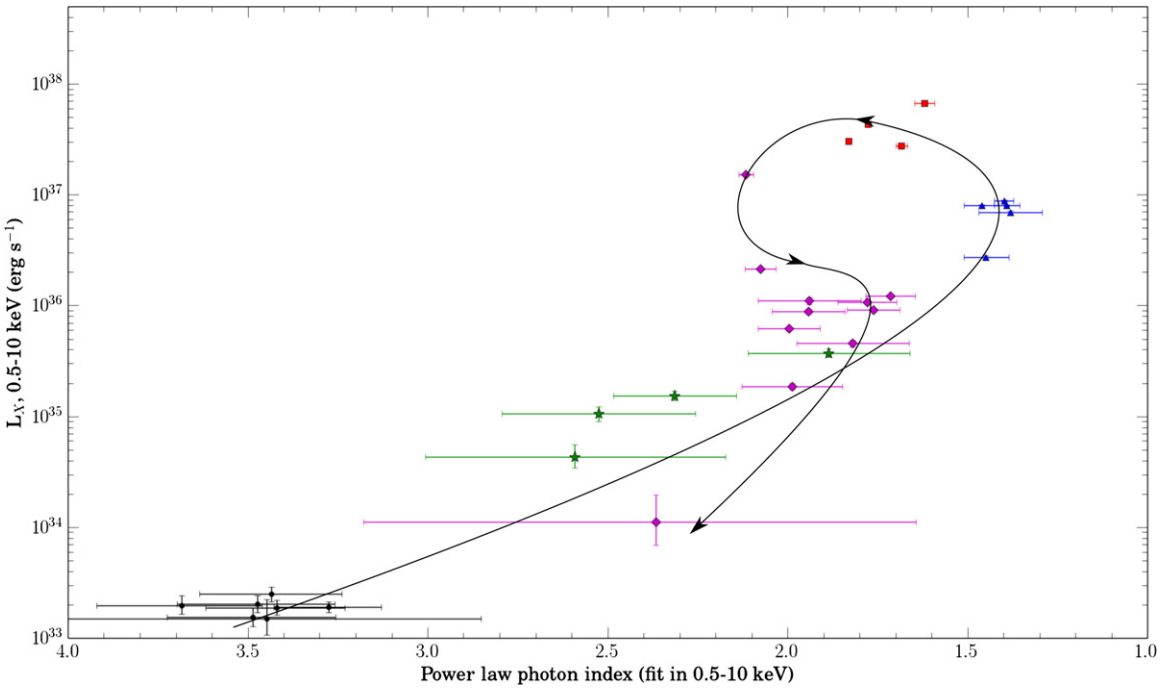

Figure 5. Luminosity vs. power-law photon index of Terzan 5 X-3 during the outburst, using *Swift*/XRT and one *Chandra*/ACIS outburst observations plus two quiescent *Chandra*/ACIS observations. Colors and shapes of points indicate the phases of outburst (as in Figure 3): (a) green stars, rise, (b) blue triangles, hard state, (c) red squares, soft state, (d) magenta diamonds, return to hard state. The black circles represent *Chandra*/ACIS observations in quiescence, covering the range of observed hardness in the quiescent state. Arrows represent the chronological order of data points. Error bars indicate 1σ uncertainties.

(A color version of this figure is available in the online journal.)

Table 2
Swift/XRT and *Chandra*/ACIS Observations Fit to an Absorbed Power-Law Model

Obs. ID	MJD	Photon Index	Flux	L_X	χ^2_ν/D.O.F.(nhp)
32148002-91445005	55966-56108	$2.4^{+0.5}_{-0.4}$	$2.4^{+0.7}_{-0.6}$	$1.0^{+0.3}_{-0.2}$	0.68/7(0.69)
91445006	56114.8	2.6 ± 0.7	10^{+5}_{-3}	4^{+2}_{-1}	0.83/6(0.54)
32148003	56115.8	2.5 ± 0.4	25^{+7}_{-5}	10^{+3}_{-2}	0.85/5(0.51)
32148004	56117.0	2.3 ± 0.3	37 ± 6	15 ± 2	1.86/9(0.052)
32148005	56118.1	1.9 ± 0.4	90 ± 12	37 ± 5	0.54/6(0.78)
32148006	56120.7	1.4 ± 0.1	658 ± 32	273 ± 13	1.58/19(0.05)
526511000	56121.7	1.4 ± 0.1	1658 ± 91	688 ± 38	1.20/14(0.27)
91445008	56124.3	1.46 ± 0.08	1920 ± 63	797 ± 26	0.69/25(0.87)
526892000	56124.9	1.39 ± 0.06	1936 ± 46	803 ± 19	1.56/34(0.03)
32148007	56125.9	1.40 ± 0.04	2125 ± 40	882 ± 17	1.05/37(0.38)
91445009[a]	56129.1	$1.8 \pm ?$	$10440 \pm ?$	$4333 \pm ?$	$3.94/56(1.9 \times 10^{-21})$
91445010	56134.1	1.62 ± 0.05	16070 ± 330	6669 ± 137	0.77/36(0.84)
13708[a](CXO)	56138.4	1.68 ± 0.03	6680 ± 80	2772 ± 33	$1.76/102(3.4 \times 10^{-6})$
91445011[a]	56140.1	$1.8 \pm ?$	$7330 \pm ?$	$3042 \pm ?$	$2.10/80(3.4 \times 10^{-6})$
91445012	56144.8	2.11 ± 0.03	3651 ± 70	1515 ± 29	1.12/38(0.27)
91445013	56149.4	2.07 ± 0.07	514 ± 20	213 ± 8	1.10/58(0.28)
32148008	56150.1	1.7 ± 0.1	295 ± 16	122 ± 7	0.81/45(0.81)
32148011	56152.2	1.8 ± 0.1	260 ± 16	108 ± 7	0.70/37(0.91)
530808000	56152.4	1.9 ± 0.2	266 ± 30	110 ± 12	1.12/10(0.34)
32148010[a]	56153.2	1.8 ± 0.1	219 ± 13	91 ± 5	$1.79/44(9.5 \times 10^{-4})$
91445014	56154.3	1.9 ± 0.2	215 ± 18	89 ± 7	1.06/23(0.38)
32148012	56158.3	2.0 ± 0.1	149 ± 11	62 ± 5	1.06/33(0.37)
91445015	56159.1	1.8 ± 0.3	110 ± 13	46 ± 5	0.97/10(0.47)
91445016	56163.2	2.0 ± 0.2	45 ± 5	19 ± 2	1.49/16(0.09)
32148013	56169.3	$2.4^{+1.5}_{-1.2}$	$2.7^{+4.8}_{-1.5}$	$1.1^{+1.9}_{-0.6}$	...

Notes. Unabsorbed flux in units of 10^{-12} erg s^{-1} cm^{-2} and luminosity in 10^{34} erg s^{-1}, both in 0.5–10 keV. All the flux and luminosity values are background subtracted. "a" indicates spectra which are not well described by a power law (null hypothesis probability is $<10^{-2}$); if $\chi^2 > 2$, no errors are calculated (indicated by "?"). The first row shows a spectral fit to a merged spectrum of 6 *Swift*/XRT observations of Terzan 5 before the outburst of Terzan 5 X-3. For Obs.ID 32148013, due to low counts, we used *cstat* statistics in the fitting. Reported uncertainties are 90% intervals.

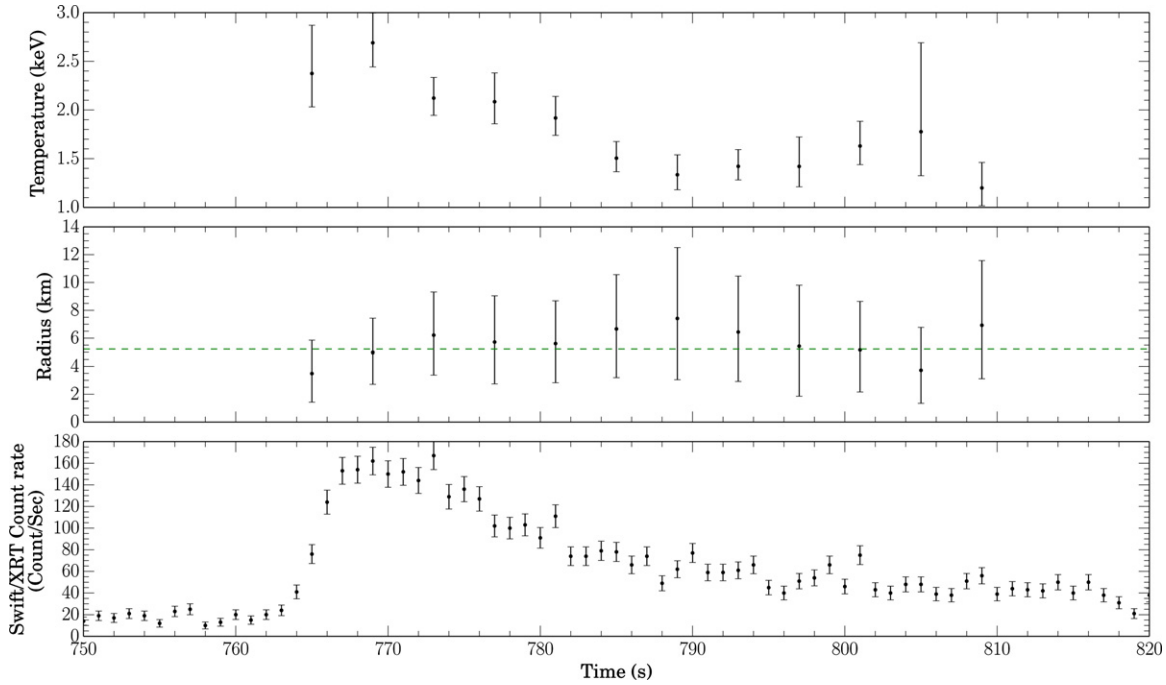

Figure 6. Spectral evolution during the thermonuclear burst of Terzan 5 X-3, using blackbody fits. The first and second panels show the variation in temperature and radius, respectively. The third panel is the 0.5–10 keV light curve of the burst. The significant drop of temperature around 770–790 s shows evidence for cooling during the thermonuclear burst. The green line in the second panel represents the weighted average radius. Error bars are 1σ uncertainties. Time bins in the top two panels are 4 s long.

(A color version of this figure is available in the online journal.)

not affect our conclusions). We fit an absorbed blackbody model (BBODYRAD) to the burst emission, finding decent fits for all intervals, and show the spectral evolution in Figure 6. We find clear evidence of cooling (between 770 and 790 s in Figure 6), while the inferred radius remains essentially constant. This is a clear signature of a thermonuclear burst, and thus of a NS.

We estimated the timescale of this burst using two methods. We fit an exponential model (count rate $\propto e^{-t/\tau_1}$) to the light curve of the burst after the peak, estimating the timescale $\tau_1 \approx 16 \pm 1$s. Following Galloway et al. (2008), we estimated an alternative timescale for thermonuclear bursts $\tau_2 = E_{\rm burst}/F_{\rm peak}$, where $E_{\rm burst}$ is the total fluence during the burst and $F_{\rm peak}$ is flux at the peak, finding $\tau_2 \approx 29$s. Galloway et al. (2008) divide bursts into those with τ_2 longer than 10 s, and those with τ_2 shorter than 10 s. The longer bursts are generally powered by hydrogen burning (with the exception of "giant" bursts involving photospheric radius expansion, which was not seen here), and the short bursts involve only helium burning, since hydrogen burning proceeds more slowly than helium burning (Fujimoto et al. 1981; van Paradijs et al. 1988; Cornelisse et al. 2003). Our measured burst timescale indicates that hydrogen is being accreted, and thus that the donor star is hydrogen-rich, which requires an orbital period $\gtrsim$1.5 hr (e.g., Nelson et al. 1986) and excludes a WD donor.

3.3.4. Quiescent Behavior

We used 7 *Chandra*/ACIS observations taken when all sources were quiescent (Table 1) to study the behavior of Terzan 5 X-3 in quiescence before its outburst. We extracted source and background spectra from each observation using CIAO *dmextract*. We used a combination of a power-law (PEGPWRLW) model and a hydrogen atmosphere for a NS (NSATMOS), with absorption (PHABS) set to our preferred cluster value, the NS radius to 10 km, mass to 1.4 $M_\odot$, and distance set to 5.9 kpc. This model has been previously used to fit its spectrum in one quiescent observation (Heinke et al. 2006b). To study possible spectral variations, we simultaneously fit spectra from each observation in four different Trials, each with different parameters free (Table 3): (I) constraining the NSATMOS and PEGPWRLW components to have the same values between all observations; (II) letting only the power-law normalization vary between observations, while constraining the NSATMOS temperature to be the same; (III) letting only the NSATMOS temperature vary between observations, while constraining the power-law normalization to be the same; (IV) letting both the power-law normalization and the NSATMOS temperature vary between observations. We found no evidence for variation in the power-law photon index Γ between observations if we allowed it to vary. Therefore, we tied its value between observations in each Trial (Figure 7).

Trial I gives a poor fit, with $\chi^2 = 116.3$ for 76 D.O.F. An F-test confirms the improvement from allowing the power-law flux to vary (Trial I to II), giving an F-statistic of 6.0 and probability of 4×10^{-5} of obtaining such an improvement by chance. Alternatively, allowing the NS temperature to vary (Trial III) also gives an improvement compared to Trial I (F-statistic of 4.2, chance improvement probability of 1×10^{-3}). Letting both components vary is a substantial improvement compared to allowing the NS temperature alone to vary (comparing III to IV, F-statistic=2.27, chance improvement probability of 4.7×10^{-2}), while letting both components vary is not preferred over allowing the power-law component alone to vary (comparing II to IV, F-statistic=0.89, chance improvement probability 0.50). Thus, we identify clear variation in the nonthermal component, but no evidence for variation in the thermal component.

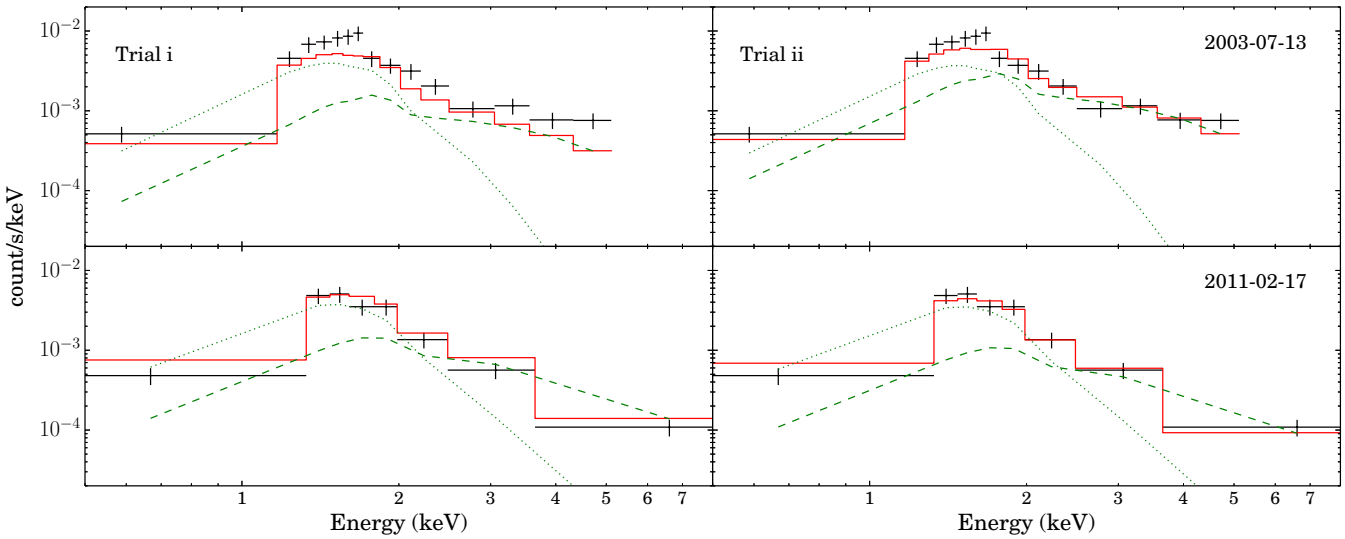

Figure 7. Extracted spectra from two of the *Chandra*/ACIS observations of Terzan 5 X-3 compared to the fitted model (NSATMOS + PEGPWRLW in XSPEC) from Trials I and II (Table 3). The dotted line indicates the contribution of the NSATMOS, while the dashed line indicates the contribution from the power-law component, and the solid line is their sum. Spectral variations are clear. Comparing Trial II to I, fitting improvement can be seen.

(A color version of this figure is available in the online journal.)

Table 3

Spectral Fitting of 7 *Chandra*/ACIS Observations of Terzan 5 X-3 During Quiescence (See Table 1), Using PHABS(PEGPWRLW+NSATMOS) in XSPEC

Trial	ObsID	log T (K)	$F_{X,\mathrm{NS}}$(0.5–10 keV) (10^{-13} erg cm^{-2} s^{-1})	Γ	$F_{X,\mathrm{PL}}$(0.5–10 keV) (10^{-13} erg cm^{-2} s^{-1})	$L_{X,\mathrm{total}}$(0.5–10 keV) (10^{33} erg s^{-1})	χ^2_ν/D.O.F.(nhp)
I	all	$6.143^{+0.015}_{-0.011}$	$2.4^{+0.3}_{-0.2}$	1.9 ± 0.4	$1.1^{+0.3}_{-0.1}$	$1.4^{+0.2}_{-0.1}$	1.53/76(0.002)
II	03798	$6.138^{+0.012}_{-0.018}$	$2.4^{+0.3}_{-0.5}$	2.1 ± 0.4	$1.9^{+0.6}_{-0.4}$	1.8 ± 0.3	1.09/70(0.27)
	10059	t	t	t	$1.3^{+0.5}_{-0.3}$	1.5 ± 0.2	t
	13225	t	t	t	$0.8^{+0.4}_{-0.3}$	1.3 ± 0.2	t
	13252	t	t	t	$1.2^{+0.5}_{-0.3}$	1.5 ± 0.2	t
	13705	t	t	t	0.7 ± 0.6	1.3 ± 0.3	t
	14339	t	t	t	$0.8^{+0.5}_{-0.3}$	1.3 ± 0.2	t
	13706	t	t	t	$1.4^{+0.4}_{-0.3}$	1.6 ± 0.2	t
III	03798	$6.172^{+0.011}_{-0.015}$	$3.3^{+0.4}_{-0.5}$	1.9 ± 0.4	$1.0^{+0.3}_{-0.2}$	1.8 ± 0.2	1.22/70(0.099)
	10059	$6.149^{+0.014}_{-0.019}$	$2.7^{+0.3}_{-0.5}$	t	t	1.5 ± 0.2	t
	13225	$6.120^{+0.019}_{-0.029}$	1.9 ± 0.5	t	t	1.2 ± 0.2	t
	13252	$6.144^{+0.014}_{-0.019}$	$2.4^{+0.3}_{-0.5}$	t	t	1.4 ± 0.2	t
	13705	$6.115^{+0.025}_{-0.042}$	$1.9^{+0.5}_{-0.7}$	t	t	1.2 ± 0.3	t
	14339	$6.131^{+0.017}_{-0.023}$	$2.2^{+0.2}_{-0.5}$	t	t	1.3 ± 0.2	t
	13706	$6.155^{+0.012}_{-0.017}$	$2.7^{+0.3}_{-0.5}$	t	t	1.5 ± 0.2	t
IV	03798	$6.161^{+0.015}_{-0.021}$	$3.0^{+0.3}_{-0.6}$	1.7 ± 0.4	1.5 ± 0.4	$1.9^{+0.2}_{-0.3}$	1.10/64(0.27)
	10059	$6.148^{+0.016}_{-0.021}$	$2.7^{+0.6}_{-0.5}$	t	$1.1^{+0.4}_{-0.3}$	$1.6^{+0.3}_{-0.2}$	t
	13225	$6.134^{+0.015}_{-0.024}$	$2.2^{+0.2}_{-0.5}$	t	$0.7^{+0.3}_{-0.2}$	1.2 ± 0.2	t
	13252	$6.146^{+0.015}_{-0.021}$	$2.7^{+0.3}_{-0.5}$	t	$1.0^{+0.4}_{-0.3}$	1.5 ± 0.2	t
	13705	$6.121^{+0.025}_{-0.043}$	1.7 ± 1.0	t	1.3 ± 0.9	1.2 ± 0.5	t
	14339	$6.142^{+0.014}_{-0.019}$	$2.4^{+0.3}_{-0.5}$	t	$0.7^{+0.4}_{-0.3}$	1.3 ± 0.2	t
	13706	$6.154^{+0.014}_{-0.021}$	$2.7^{+0.3}_{-0.5}$	t	$1.1^{+0.3}_{-0.2}$	1.6 ± 0.2	t

Notes. In Trial I both components are constrained to have the same values between observations. In Trials II and III one of the components may vary between observations, while in Trial IV both components are free. We use a "t" whenever values of a parameter are tied between observations. kT is the NS surface temperature in the star's frame, Γ is the power-law photon index, $F_{X,\mathrm{NS}}$ is the unabsorbed flux from the NS atmosphere component, and $F_{X,\mathrm{PL}}$ is the unabsorbed flux from the power-law component. Uncertainties are 90% confidence intervals. nhp is the null hypothesis probability (otherwise known as the p-value).

3.3.5. Rise of the Outburst

We fit the *Swift*/XRT spectra from the rise of the outburst with a two-component model including a thermal component (BBODYRAD in XSPEC) and a nonthermal component (PEGPWRLW in XSPEC). We found good fits permitting only the relative normalizations of the thermal and nonthermal components to vary, with a photon index tied between observations ($\Gamma = 1.1^{+0.2}_{-0.4}$) and a blackbody radius tied between observations ($R = 4.3^{+1.4}_{-1.2}$ km). When the power-law index is left free between observations, the values are consistent, though they

Table 4
Results of Spectral Analyses for the Rise of the Outburst with a Two-Component Model: Thermal (BBODYRAD in XSPEC) Plus Nonthermal (PEGPWRLW in XSPEC)

Obs. ID	MJD	kT (keV)	$F_{X,\mathrm{BB}}$ (0.5–10 keV) (10^{-12} erg s^{-1} cm^{-2})	$F_{X,\mathrm{PL}}$ (0.5–10 keV) (10^{-12} erg s^{-1} cm^{-2})	$F_{X,\mathrm{PL}}/F_{X,\mathrm{total}}$	$L_{X,\mathrm{total}}$(0.5–10 keV) (10^{34} erg s^{-1})	χ^2_ν/D.O.F.
91445006	56114.8	0.31 ± 0.03	5 ± 2	5 ± 2	$50 \pm 20\%$	4 ± 1	0.53/6
32148003	56115.8	0.36 ± 0.03	9 ± 3	13 ± 4	$59^{+15}_{-16}\%$	9 ± 2	0.68/5
32148004	56117	0.41 ± 0.02	15^{+4}_{-3}	17 ± 6	$53^{+12}_{-16}\%$	13 ± 3	1.19/9
32148005	56118.1	$0.44^{+0.05}_{-0.07}$	20 ± 10	70 ± 20	$78^{+12}_{-15}\%$	37 ± 9	0.55/6
32148006	56120.7	0.67 ± 0.06	110 ± 40	500^{+60}_{-70}	$82^{+7}_{-8}\%$	250 ± 30	1.39/19

Notes. $F_{X,\mathrm{BB}}$ and $F_{X,\mathrm{PL}}$ are the blackbody and power-law unabsorbed fluxes, respectively. The power-law photon index was tied between spectra and was found to be $1.1^{+0.2}_{-0.4}$. The thermal component normalization (which is proportional to blackbody radius) is assumed constant and is tied between observations. Uncertainties are 90% confidence intervals. χ^2_ν and degrees of freedom in this table are found by fitting each data set individually based on values found in simultaneous fit.

are poorly constrained in several spectra. Comparing our two-component model fits (Table 4) to our power-law fits (Table 2), a clear improvement in the fit is seen. Simultaneous fits to the first five *Swift*/XRT spectra of the outburst (listed in Table 4) with an absorbed power-law (with the photon index free between observations) give a reduced χ^2 of 1.32 for 45 degrees of freedom, while fits with an absorbed power-law plus blackbody give a reduced χ^2 of 1.09 for 43 degrees of freedom. An F-test gives an F-statistic of 5.55 and chance improvement probability of 0.007, supporting the addition of the thermal component. Protassov et al. (2002) showed that the F-test is often inaccurate for testing the necessity of adding an additional spectral component. We therefore chose the spectrum with the clearest evidence of a thermal component (ObsID 32148004), which shows a $\Delta\chi^2$ of 6.1 between the power-law and power-law plus thermal spectral fits (going from 12 degrees of freedom to 11). We simulated 1000 data sets using a best-fit absorbed power-law model, and fit them both with a power-law model and with a power-law plus thermal component model. None of our simulations showed a larger $\Delta\chi^2$ than that produced by our model, allowing us to conclude that the probability of incorrectly concluding that a thermal component is required is less than 99.5%.

This indicates that the hardening during the outburst rise is likely caused by the decreasing relative contribution of a thermal component. With increasing time, and thus with increasing L_x, the fractional contribution of the thermal component decreases, but its kT increases monotonically. In the next section, we suggest that the thermal component is due to low-level accretion onto the surface of the NS.

4. DISCUSSION

4.1. Hardening during the Outburst Rise

We observed clear evidence of hardening of the spectrum during the outburst rise from $L_X \sim 4 \times 10^{34}$ up to 10^{36} erg s^{-1}. We have evidence that this hardening is due to the relative reduction in strength of a thermal component in the spectrum with increasing brightness. This is the first time that such hardening during the outburst rise has been detected, made possible by our program of *Swift*/XRT globular cluster monitoring allowing early detection of the outburst below $L_X = 10^{35}$ erg s^{-1}. The trend of inferred photon index (for a fit to a power-law model) versus L_X is clear from the data in the rise, and is consistent with the data in the decay (which are not well-sampled below $L_X = 10^{35}$ erg s^{-1}); see Figure 5.

Softening during outburst decays has been seen from other (likely) NS LMXBs, in the L_X range of $10^{34} - 10^{35.5}$ erg s^{-1}, especially when the soft (<2 keV) X-ray energy range is included (Jonker et al. 2003, 2004; Cackett et al. 2011; Fridriksson et al. 2011; Armas Padilla et al. 2011, 2013c). *RXTE* observations have shown marginal softening during the decay of Aql X-1 down to $L_X = 5 \times 10^{34}$ erg s^{-1} (Maitra & Bailyn 2004), only in the part of the spectrum below 6 keV. *RXTE* observations of SAX J1808.4-3658 showed almost no spectral changes from $L_X \sim 2 \times 10^{36}$ down to 2×10^{34} erg s^{-1} (Gilfanov et al. 1998). These apparently contrasting observations are consistent if the softening is due to the increasing importance of the thermal component at lower L_X. Evidence in favor of an increasing relative thermal component can also be seen in *Swift*/XRT spectra of SAX J1808.4-3658 declining from $L_X \sim 10^{36}$ down to 10^{33} erg s^{-1} (Campana et al. 2008). Thus, we interpret the hardening we observe in Terzan 5 X-3's rise as due primarily to the decreasing importance of a thermal component, rather than to the same physics responsible for the softening of black hole LMXBs during their decay, which show a steepening power-law spectrum (e.g., Plotkin et al. 2013).

Comparing the spectra observed from Terzan 5 X-3 to those of other NS LMXBs, we find a common pattern, that below $L_X \sim 1$–3×10^{35} erg s^{-1} a thermal component is often required. For instance, Armas Padilla et al. (2013b) find, using XMM-Newton spectra, that two LMXBs at $L_X = 1$–10×10^{34} erg s^{-1} require a strong thermal component, while this is not critical for another LMXB at $L_X \sim 10^{35}$ erg s^{-1}. Wijnands et al. (2002b), using *Chandra* find that SAX J1747.0-2853, at $L_X \sim 3 \times 10^{35}$ erg s^{-1}, does not need a thermal component. Armas Padilla et al. (2013c) measure a thermal component to comprise ~20% of the 0.5–10 keV luminosity for a transient at $L_X \sim 9 \times 10^{34}$ erg s^{-1} (using XMM), with no evidence (from poorer *Swift*/XRT spectra) for a thermal component above $L_X = 2.6 \times 10^{35}$ erg s^{-1}. Jonker et al. (2003, 2004) study the return to quiescence of XTE J1709-267, finding a thermal component to comprise ~40% of the flux at $L_X \sim 4 \times 10^{34}$ erg s^{-1}, increasing to >90% at 2×10^{33} erg s^{-1}. All these results suggest that there is a physical transition operating around $L_X \sim 10^{35}$ erg s^{-1} which changes the energy spectra.

Such a transition can be provided by the declining optical depth of a hot Comptonizing atmosphere, as seen in numerical calculations of NSs accreting at low rates (Deufel et al. 2001; Popham & Sunyaev 2001). Deufel et al. 2001 show temperature profiles and emergent spectra for NSs illuminated by high-temperature protons, such as are produced by radiatively inefficient accretion flows. In their Figures 4 and 5 they show that the emergent spectrum is a featureless Comptonized spectrum extending to ~100 keV above $L_X \sim 10^{36}$ erg s^{-1}, which develops a clear 0.5 keV thermal component at ~10^{35} erg s^{-1},

Table 5
Orbital Periods, or Other Classification, of the 18 Galactic Globular Cluster LMXBs That Are Persistently Bright or Have Shown Luminous Outbursts Plus Three Quiescent Globular Cluster LMXBs

LMXB	Globular Cluster	State	P_{orb}	Nature	Notes	References
4U 1820-30	NGC 6624	P	11 min	U	X	(1)
4U 0513-40	NGC 1851	P	17 min	U	UV	(2)
X1850-087	NGC 6712	P	20.6[a] min	U	UV	(3)
M15 X-2	M 15	P	22.6 min	U	UV	(4)
NGC 6440 X-2	NGC 6440	T	57.3 min	U	XP	(5)
XB 1832-330	NGC 6652	P	2.1 hr	N	O	(6)
4U 1746-37	NGC 6441	P	5.16 hr	N	X	(7)
SAX J1748.9-2021	NGC 6440	T	8.7 hr	N	XP	(8)
IGR J18245-2452	M28	T	11.0 hr	N	XP	(9)
GRS 1747-312	Terzan 6	T	12.36 hr	N	X	(10)
AC 211	M 15	P	17.1 hr	N	UV	(11)
Terzan 5 X-2	Terzan 5	T	21.27 hr	N	XP	(12, 13)
Rapid Burster	Liller 1	T	?	N	B	(14)
EXO 1745-248	Terzan 5	T	?	N	B	(14)
Terzan 5 X-3	Terzan 5	T	?	N	B	(15)
XB 1732-304	Terzan 1	T	?	?	?	(16)
4U 1722-30	Terzan 2	P	?	U?	B	(17)
IGR J17361-4441	NGC 6388	T	?	?	?	(18)
LMXBs with no observed outbursts						
47 Tuc W37	47 Tuc	Q	3.09 hr	N	X	(19)
47 Tuc X5	47 Tuc	Q	8.67 hr	N	X	(20)
ω Cen qLMXB	ω Cen	Q	?	N	Hα	(21)

Notes. X-ray bursts have been detected from all the bright LMXBs except for AC 211 in M15 and IGR J17361-4441 in NGC 6388. State: P = persistent (or active for >30 yr), T = transient, Q = quiescent (so far). Nature: U = ultracompact, N = normal. Notes: X = period from X-ray photometry, UV = period from UV photometry, XP = period from X-ray pulsations, O = period from optical photometry, B = nature of donor inferred from properties of X-ray bursts, Hα = hydrogen seen in optical counterpart spectrum. Notes represent method of measuring P_{orb} or determining donor nature.
References. (1) Stella et al. 1987; (2) Zurek et al. 2009; (3) Homer et al. 1996; (4) Dieball et al. 2005; (5) Altamirano et al. 2010; (6) Engel et al. 2012; (7) Bałucińska-Church et al. 2004; (8) Altamirano et al. 2008; (9) Papitto et al. 2013; (10) in't Zand et al. 2003; (11) Ilovaisky et al. 1993; (12) Strohmayer et al. 2010; (13) Papitto et al. 2011; (14) Galloway et al. 2008; (15) this work; (16) Guainazzi et al. 1999; (17) in't Zand et al. 2007; (18) Bozzo et al. 2011; (19) Heinke et al. 2005; (20) Heinke et al. 2003b; (21) Haggard et al. 2004.
[a] Or the alias period of 13 minutes.

and loses the Comptonized tail by 10^{33} erg s^{-1}. This transition is a strikingly accurate match to our observations of Terzan 5 X-3's spectral variations, and to other NS transients discussed in the literature. However calculations of Deufel et al. 2001 underpredict the observed hard power-law components seen in many quiescent LMXBs at low L_X ($<10^{34}$ erg s^{-1}, including Terzan 5 X-3 in quiescence). This may arise from their not including the Comptonizing effects of the overlying accretion flow on the observed spectrum. Popham & Sunyaev (2001) compute solutions for a hot boundary layer, which becomes optically thin for accretion luminosities below $\sim 10^{36}$ erg s^{-1}, suggesting that some additional Comptonization can be performed by the accretion flow.

The temperature of the thermal component increases monotonically with the total X-ray luminosity during the rise (Table 4), as expected if the thermal component during the rise is produced by accretion. A correlation of thermal component temperature with total luminosity has been suggested from comparisons of multiple sources (Armas Padilla et al. 2013c), but this measurement clearly confirms this correlation in a single source. Furthermore, heating of the NS crust by accretion during the outburst will give rise to a rapidly decaying surface temperature at the end of the outburst (e.g., Cackett et al. 2006b). This effect of an accretion-heated crust could be confused with changing thermal emission from low-level accretion onto the NS surface during the outburst decline, but is not an issue during the outburst rise.

4.2. Nature of Donors in Globular Cluster X-Ray Binaries

The detection of a thermonuclear burst during this outburst showed that the accreting object is a NS. Furthermore, the timescale of this thermonuclear burst indicates that the accreted matter contains hydrogen, evidence that the donor is not a white dwarf. With this information, we are now capable of classifying 15 of the 18 known bright Galactic globular cluster LMXBs as either ultracompact ($P_{orb} < 1$ hr, accreting from a hydrogen-deficient and/or degenerate donor) or not ultracompact (accreting from a nondegenerate, H-rich star). Five are known to be ultracompact by direct detection of their orbital periods, and seven systems are known not to be ultracompact by direct measurement of their orbital periods. On the basis of X-ray burst behavior indicative of hydrogen burning (Galloway et al. 2008), another three systems can be identified as not ultracompact (Table 5). (4U 1722-30, in Terzan 2, has shown some evidence, by its persistent low-luminosity accretion and burst behavior, in favor of an ultracompact nature; in't Zand et al. 2007.) Thus, the fraction of observed bright globular cluster LMXBs that are ultracompact appears to be between 28 and 44% (for 5 or 8 of 18). This fraction is believed to be higher than in the rest of the Galaxy (Deutsch et al. 2000), but uncertainties in selection effects mean that we cannot confidently extrapolate the true underlying fraction of ultracompact systems and make clear comparisons to binary population synthesis models (e.g., Ivanova et al. 2008).

4.3. Quiescent Counterpart

We have identified the quiescent counterpart to Terzan 5-X3 with the brightest previously suggested candidate quiescent LMXB in the cluster, CXOGLB J174805.4-244637 (Heinke et al. 2006b). Our spectral analysis reveals evidence for a variable power-law contribution to the quiescent spectrum over timescales of years, but exhibits no evidence for changes to the thermal component. It is fascinating to see clearly here that the quiescent spectral properties appear to lie on a continuum with the outburst properties, with increasing hardening from quiescence, through the early rise, up to the hard state at $L_X > 10^{36}$ erg s^{-1} (Figure 5).

Chandra quiescent X-ray counterpart searches have now been performed for nine transient cluster LMXBs, of which the three with the faintest outbursts have been identified with very faint ($L_X < 10^{32}$ erg s^{-1}) quiescent counterparts (M15 X-3, Heinke et al. 2009; NGC 6440 X-2, Heinke et al. 2010; IGR J17361-4441 in NGC 6388, Pooley et al. 2011b), two have spectrally hard counterparts with $L_X \sim 10^{32}$–10^{33} erg s^{-1} (EXO 1745-248 in Terzan 5, Wijnands et al. 2005; IGR J18245-2452 in M28, Papitto et al. 2013; Linares et al. 2013), and four have spectrally soft counterparts with $L_X \sim 10^{32}$–10^{33} erg s^{-1} (SAX J1748.9-2021 in NGC 6440, in't Zand et al. 2001; X1732-304 in Terzan 1, Cackett et al. 2006a; IGR J17480-2446 in Terzan 5, Degenaar & Wijnands 2011; and Terzan 5 X-3). These identifications support the idea that the faint soft X-ray sources identified as candidate quiescent LMXBs in globular clusters are indeed transient LMXBs, between (relatively bright) outbursts (Heinke et al. 2003c; Wijnands et al. 2013). The brightest of the faint soft X-ray sources should experience relatively high long-term average mass accretion rates, which will cause relatively large amounts of deep crustal heating and keep their cores warm. Such high mass accretion rates suggest frequent outbursts, and thus it is comforting that we have identified the brightest of the faint soft X-ray sources in the clusters NGC 6440, Terzan 5, and Terzan 1 with observed transients. The suggestion that roughly half the quiescent LMXBs in each cluster are easily identifiable in short *Chandra* observations by showing soft, primarily thermal X-ray spectra and X-ray luminosities between 10^{32} and 10^{33} erg s^{-1} (Heinke et al. 2005) continues to seem reasonable, though it remains unproven.

From the quiescent NS thermal bolometric luminosity ($L_{\rm NS,(0.01-10\,keV)} = 1.5 \times 10^{33}$ erg s^{-1}, $kT = 118$ eV at the surface) of Terzan 5 X-3, and its outburst properties, we can make some general statements about its outburst history or neutrino cooling properties, assuming that the quiescent thermal flux is due to heat deposited in the core during multiple accretion episodes (Brown et al. 1998). We estimate the total mass transfer rate onto the NS during this outburst by converting the daily *MAXI*/GSC 4–10 keV flux estimates (in Crab units) into 0.1–12 keV fluxes (assuming a power-law with photon index set by the nearest *Swift*/XRT observations), converting the daily *Swift*/BAT flux estimates into 12–50 keV fluxes (using the same power-law photon index as for the *MAXI* data), adding these together, and assuming a 1.4 $M_\odot$, 10 km NS. This gives us a total energy release over the outburst of 9×10^{43} erg, and a total mass transfer of 2.4×10^{-10} $M_\odot$.

If we assume "standard" modified Urca cooling (Yakovlev & Pethick 2004; Wijnands et al. 2013), then we can estimate (using the quiescent NS luminosity) a mass transfer rate onto the NS of $\dot{M} \sim 3 \times 10^{-11}$ $M_\odot$ yr^{-1} (though this value might vary depending on the choice of crustal composition, e.g., whether a thick light-element layer is present; Page et al. 2004). Assuming this outburst is typical, we derive an average interval of ~8 yr between outbursts. If the average interval between outbursts were much longer than 10 yr, then Terzan 5 X-3 would be brighter in quiescence than expected under even the slowest cooling processes. One could attribute its quiescent thermal luminosity to continued accretion, but our analysis of the quiescent observations identifies no evidence for variability in the thermal component, arguing against this explanation. All Terzan 5 X-ray outbursts since 1996 have been identified with their quiescent counterpart with arcsecond precision, except one in 2002 (Wijnands et al. 2002a). The 2002 outburst had an average luminosity of $L_X \sim 2 \times 10^{37}$ erg s^{-1}, peak $L_X \sim 4 \times 10^{37}$ erg s^{-1}, and lasted for ~30 days (Degenaar & Wijnands 2012). The 2012 outburst of Terzan 5 X-3 had a similar average luminosity of $L_X \sim 2 \times 10^{37}$ erg s^{-1}, peak $L_X = 7 \times 10^{37}$ erg s^{-1}, and lasted for 30 days above $L_X \sim 10^{36}$ erg s^{-1} (comparable to the RXTE/ASM detection limit for the 2002 outburst). We therefore suggest that the 2002 X-ray outburst is likely to have also been produced by Terzan 5 X-3. This would nicely fit the ~8 yr recurrence time we inferred above.

We thank H. A. Krimm for helpful discussion on the analysis of *Swift*/BAT survey data, and T. Mihara for helpful discussion on *MAXI*/GSC calibration issues. We acknowledge financial support from NSERC Discovery Grants (C.O.H., G.R.S.), an Alberta Ingenuity New Faculty Award (C.O.H.) and the Avadh Bhatia Fellowship (J.C.G.). N.D. is supported by NASA through Hubble Postdoctoral Fellowship grant number HST-HF-51287.01-A from the Space Telescope Science Institute. R.W. is supported by an European Research Council Starting Grant. D.A. acknowledges support from the Royal Society. J.H. and D.P. acknowledge support by the National Aeronautics and Space Administration through Chandra Award Number GO2-13045B, issued by the Chandra X-Ray Observatory Center, which is operated by the Smithsonian Astrophysical Observatory for and on behalf of the National Aeronautics Space Administration under contract NAS8-03060.

This research has made use of the following data and software packages: observations made by the *Chandra X-Ray Observatory*, data obtained from the Chandra Data Archive, software provided by the Chandra X-Ray Center (CXC) in the application package CIAO, *MAXI* data provided by RIKEN, JAXA and the MAXI team, *Swift*/BAT transient monitor results provided by the *Swift*/BAT team, and the *Swift*/XRT Data Analysis Software (XRTDAS) developed under the responsibility of the ASI Science Data Center (ASDC), Italy. We acknowledge extensive use of the ADS and arXiv.

Facilities: CXO (ACIS), Swift (XRT, BAT), MAXI (GSC)

REFERENCES

Altamirano, D., Casella, P., Patruno, A., Wijnands, R., & van der Klis, M. 2008, ApJL, 674, L45
Altamirano, D., Ingram, A., van der Klis, M., et al. 2012a, ApJL, 759, L20
Altamirano, D., Keek, L., Cumming, A., et al. 2012b, MNRAS, 426, 927
Altamirano, D., Patruno, A., Markwardt, C. B., et al. 2010, ApJL, 712, L58
Altamirano, D., Wijnands, R., Heinke, C. O., Sivakoff, G. R., & Pooley, D. 2012c, ATel, 4264, 1
Anders, E., & Grevesse, N. 1989, GeCoA, 53, 197
Armas Padilla, M., Degenaar, N., Patruno, A., et al. 2011, MNRAS, 417, 659
Armas Padilla, M., Degenaar, N., Russell, D. M., & Wijnands, R. 2013a, MNRAS, 428, 3083

Armas Padilla, M., Degenaar, N., & Wijnands, R. 2013b, MNRAS, 436, L89
Armas Padilla, M., Wijnands, R., & Degenaar, N. 2013c, MNRAS, submitted (arXiv:1307.6009)
Arnaud, K. A. 1996, in ASP Conf. Ser. 101, Astronomical Data Analysis Software and Systems V, ed. G. H. Jacoby & J. Barnes (San Francisco, CA: ASP), 17
Bahramian, A., Heinke, C. O., Sivakoff, G. R., & Gladstone, J. C. 2013, ApJ, 766, 136
Bałucińska-Church, M., Church, M. J., & Smale, A. P. 2004, MNRAS, 347, 334
Barthelmy, S. D., Barbier, L. M., Cummings, J. R., et al. 2005, SSRv, 120, 143
Blackburn, J. K. 1995, in ASP Conf. Ser. 77, Astronomical Data Analysis Software and Systems IV, ed. R. A. Shaw, H. E. Payne, & J. J. E. Hayes (San Francisco, CA: ASP), 367
Bordas, P., Kuulkers, E., Alfonso-Garzón, J., et al. 2010, ATel, 2919, 1
Bozzo, E., Ferrigno, C., Stevens, J., et al. 2011, A&A, 535, L1
Brown, E. F., Bildsten, L., & Rutledge, R. E. 1998, ApJL, 504, L95
Burrows, D. N., Hill, J. E., Nousek, J. A., et al. 2005, SSRv, 120, 165
Cackett, E. M., Brown, E. F., Miller, J. M., & Wijnands, R. 2010, ApJ, 720, 1325
Cackett, E. M., Fridriksson, J. K., Homan, J., Miller, J. M., & Wijnands, R. 2011, MNRAS, 414, 3006
Cackett, E. M., Wijnands, R., Heinke, C. O., et al. 2006a, MNRAS, 369, 407
Cackett, E. M., Wijnands, R., Linares, M., et al. 2006b, MNRAS, 372, 479
Campana, S., Colpi, M., Mereghetti, S., Stella, L., & Tavani, M. 1998, A&ARv, 8, 279
Campana, S., Israel, G. L., Stella, L., Gastaldello, F., & Mereghetti, S. 2004, ApJ, 601, 474
Campana, S., Stella, L., & Kennea, J. A. 2008, ApJL, 684, L99
Cavecchi, Y., Patruno, A., Haskell, B., et al. 2011, ApJL, 740, L8
Chakraborty, M., Bhattacharyya, S., & Mukherjee, A. 2011, MNRAS, 418, 490
Corbel, S., Koerding, E., & Kaaret, P. 2008, MNRAS, 389, 1697
Corbel, S., Tomsick, J. A., & Kaaret, P. 2006, ApJ, 636, 971
Cornelisse, R., in't Zand, J. J. M., Verbunt, F., et al. 2003, A&A, 405, 1033
D'Antona, F., Ventura, P., Caloi, V., et al. 2010, ApJL, 715, L63
Degenaar, N., Brown, E. F., & Wijnands, R. 2011, MNRAS, 418, L152
Degenaar, N., & Wijnands, R. 2011, MNRAS, 412, L68
Degenaar, N., & Wijnands, R. 2012, MNRAS, 422, 581
Degenaar, N., Wijnands, R., Brown, E. F., et al. 2013a, ApJ, 775, 48
Degenaar, N., Wijnands, R., & Miller, J. M. 2013b, ApJL, 767, L31
Deufel, B., Dullemond, C. P., & Spruit, H. C. 2001, A&A, 377, 955
Deutsch, E. W., Margon, B., & Anderson, S. F. 2000, ApJL, 530, L21
Dieball, A., Knigge, C., Zurek, D. R., et al. 2005, ApJL, 634, L105
Done, C., Gierliński, M., & Kubota, A. 2007, A&ARv, 15, 1
Engel, M. C., Heinke, C. O., Sivakoff, G. R., Elshamouty, K. G., & Edmonds, P. D. 2012, ApJ, 747, 119
Esin, A. A., McClintock, J. E., & Narayan, R. 1997, ApJ, 489, 865
Fender, R. P., Belloni, T. M., & Gallo, E. 2004, MNRAS, 355, 1105
Ferraro, F. R., Dalessandro, E., Mucciarelli, A., et al. 2009, Natur, 462, 483
Fridriksson, J. K., Homan, J., Wijnands, R., et al. 2011, ApJ, 736, 162
Fruscione, A., McDowell, J. C., Allen, G. E., et al. 2006, Proc. SPIE, 6270, 62701V
Fujimoto, M. Y., Hanawa, T., & Miyaji, S. 1981, ApJ, 247, 267
Galloway, D. K., Muno, M. P., Hartman, J. M., Psaltis, D., & Chakrabarty, D. 2008, ApJS, 179, 360
Gardner, E., & Done, C. 2012, MNRAS, 434, 3454
Gierliński, M., & Done, C. 2002, MNRAS, 337, 1373
Gilfanov, M., Revnivtsev, M., & Molkov, S. 2003, A&A, 410, 217
Gilfanov, M., Revnivtsev, M., Sunyaev, R., & Churazov, E. 1998, A&A, 338, L83
Gladstone, J., Done, C., & Gierliński, M. 2007, MNRAS, 378, 13
Guainazzi, M., Parmar, A. N., & Oosterbroek, T. 1999, A&A, 349, 819
Güver, T., & Özel, F. 2009, MNRAS, 400, 2050
Haggard, D., Cool, A. M., Anderson, J., et al. 2004, ApJ, 613, 512
Harris, W. E. 1996, AJ, 112, 1487
Hasinger, G., & van der Klis, M. 1989, A&A, 225, 79
Heinke, C. O., Altamirano, D., Cohn, H. N., et al. 2010, ApJ, 714, 894
Heinke, C. O., Cohn, H. N., & Lugger, P. M. 2009, ApJ, 692, 584
Heinke, C. O., Edmonds, P. D., Grindlay, J. E., et al. 2003a, ApJ, 590, 809
Heinke, C. O., Grindlay, J. E., & Edmonds, P. D. 2005, ApJ, 622, 556
Heinke, C. O., Grindlay, J. E., Lloyd, D. A., & Edmonds, P. D. 2003b, ApJ, 588, 452
Heinke, C. O., Grindlay, J. E., Lugger, P. M., et al. 2003c, ApJ, 598, 501
Heinke, C. O., Rybicki, G. B., Narayan, R., & Grindlay, J. E. 2006a, ApJ, 644, 1090
Heinke, C. O., Wijnands, R., Altamirano, D., Pooley, D., & Sivakoff, G. R. 2012, ATel, 4249, 1
Heinke, C. O., Wijnands, R., Cohn, H. N., et al. 2006b, ApJ, 651, 1098
Hessels, J. W. T., Ransom, S. M., Stairs, I. H., et al. 2006, Sci, 311, 1901
Homan, J., & Pooley, D. 2012, ATel, 4302, 1
Homer, L., Charles, P. A., Naylor, T., et al. 1996, MNRAS, 282, L37
Ilovaisky, S. A., Auriere, M., Koch-Miramond, L., et al. 1993, A&A, 270, 139
in't Zand, J. J. M., Cumming, A., van der Sluys, M. V., Verbunt, F., & Pols, O. R. 2005, A&A, 441, 675
in't Zand, J. J. M., Hulleman, F., Markwardt, C. B., et al. 2003, A&A, 406, 233
in't Zand, J. J. M., Jonker, P. G., & Markwardt, C. B. 2007, A&A, 465, 953
in't Zand, J. J. M., van Kerkwijk, M. H., Pooley, D., et al. 2001, ApJL, 563, L41
Ivanova, N., Heinke, C. O., Rasio, F. A., Belczynski, K., & Fregeau, J. M. 2008, MNRAS, 386, 553
Jonker, P. G., Galloway, D. K., McClintock, J. E., et al. 2004, MNRAS, 354, 666
Jonker, P. G., Méndez, M., Nelemans, G., Wijnands, R., & van der Klis, M. 2003, MNRAS, 341, 823
Krimm, H. A., Holland, S. T., Corbet, R. H. D., et al. 2013, ApJS, 209, 14
Lanzoni, B., Ferraro, F. R., Dalessandro, E., et al. 2010, ApJ, 717, 653
Lasota, J.-P. 2001, NewAR, 45, 449
Lewin, W. H. G., van Paradijs, J., & Taam, R. E. 1993, SSRv, 62, 223
Lin, D., Remillard, R. A., & Homan, J. 2007, ApJ, 667, 1073
Linares, M., Altamirano, D., Chakrabarty, D., Cumming, A., & Keek, L. 2012, ApJ, 748, 82
Linares, M., Chakrabarty, D., & van der Klis, M. 2011, ApJL, 733, L17
Linares, M., et al. 2013, MNRAS, in press
Maitra, D., & Bailyn, C. D. 2004, ApJ, 608, 444
Makishima, K., Ohashi, T., Inoue, H., et al. 1981, ApJL, 247, L23
Massari, D., Mucciarelli, A., Dalessandro, E., et al. 2012, ApJL, 755, L32
Matsuoka, M., Kawasaki, K., Ueno, S., et al. 2009, PASJ, 61, 999
Mihara, T., Nakajima, M., Sugizaki, M., et al. 2011, PASJ, 63, 623
Miller, J. M., Cackett, E. M., & Reis, R. C. 2009, ApJL, 707, L77
Miller, J. M., Maitra, D., Cackett, E. M., Bhattacharyya, S., & Strohmayer, T. E. 2011, ApJL, 731, L7
Motta, S., D'Aı, A., Papitto, A., et al. 2011, MNRAS, 414, 1508
Nelson, L. A., Rappaport, S. A., & Joss, P. C. 1986, ApJ, 304, 231
Page, D., Lattimer, J. M., Prakash, M., & Steiner, A. W. 2004, ApJS, 155, 623
Papitto, A., D'Aì, A., Motta, S., et al. 2011, A&A, 526, L3
Papitto, A., Di Salvo, T., Burderi, L., et al. 2012, MNRAS, 423, 1178
Papitto, A., Ferrigno, C., Bozzo, E., et al. 2013, Natur, 501, 517
Patruno, A., Bult, P., Gopakumar, A., et al. 2012, ApJL, 746, L27
Peng, F., Brown, E. F., & Truran, J. W. 2007, ApJ, 654, 1022
Plotkin, R. M., Gallo, E., & Jonker, P. G. 2013, ApJ, 773, 59
Pooley, D., Homan, J., Altamirano, D., et al. 2011a, ATel, 3743, 1
Pooley, D., Homan, J., Heinke, C., et al. 2010, ATel, 2974, 1
Pooley, D., Homan, J., Heinke, C. O., et al. 2011b, ATel, 3627, 1
Popham, R., & Sunyaev, R. 2001, ApJ, 547, 355
Protassov, R., van Dyk, D. A., Connors, A., Kashyap, V. L., & Siemiginowska, A. 2002, ApJ, 571, 545
Pszota, G., Zhang, H., Yuan, F., & Cui, W. 2008, MNRAS, 389, 423
Rajagopal, M., & Romani, R. W. 1996, ApJ, 461, 327
Ransom, S. M., Hessels, J. W. T., Stairs, I. H., et al. 2005, Sci, 307, 892
Remillard, R. A., & McClintock, J. E. 2006, ARA&A, 44, 49
Riggio, A., Burderi, L., Di Salvo, T., et al. 2012, ApJL, 754, L11
Romano, P., Campana, S., Chincarini, G., et al. 2006, A&A, 456, 917
Rutledge, R. E., Bildsten, L., Brown, E. F., Pavlov, G. G., & Zavlin, V. E. 2002, ApJ, 577, 346
Serino, M., Mihara, T., Matsuoka, M., et al. 2012, PASJ, 64, 91
Sivakoff, G. R., Jordán, A., Sarazin, C. L., et al. 2007, ApJ, 660, 1246
Stella, L., Priedhorsky, W., & White, N. E. 1987, ApJL, 312, L17
Strohmayer, T. E., & Markwardt, C. B. 2010, ATel, 2929, 1
Strohmayer, T. E., Markwardt, C. B., Pereira, D., & Smith, E. A. 2010, ATel, 2946, 1
Testa, V., di Salvo, T., D'Antona, F., et al. 2012, A&A, 547, A28
Titarchuk, L. 1994, ApJ, 434, 570
Valenti, E., Ferraro, F. R., & Origlia, L. 2007, AJ, 133, 1287
van Paradijs, J., Penninx, W., & Lewin, W. H. G. 1988, MNRAS, 233, 437
Verbunt, F., Bunk, W., Hasinger, G., & Johnston, H. M. 1995, A&A, 300, 732
Verbunt, F., & Hut, P. 1987, in IAU Symp. 125, The Origin and Evolution of Neutron Stars, ed. D. J. Helfand & J.-H. Huang (Dordrecht: Reidel), 187
Warwick, R. S., Norton, A. J., Turner, M. J. L., Watson, M. G., & Willingale, R. 1988, MNRAS, 232, 551
White, N. E., & Angelini, L. 2001, ApJL, 561, L101
Wijnands, R., Altamirano, D., Heinke, C. O., Sivakoff, G. R., & Pooley, D. 2012, ATel, 4242, 1
Wijnands, R., Degenaar, N., & Page, D. 2013, MNRAS, 432, 2366
Wijnands, R., Heinke, C. O., Pooley, D., et al. 2005, ApJ, 618, 883

Wijnands, R., Homan, J., & Remillard, R. 2002a, ATel, 101, 1
Wijnands, R., Miller, J. M., & Wang, Q. D. 2002b, ApJ, 579, 422
Wilms, J., Allen, A., & McCray, R. 2000, ApJ, 542, 914
Worpel, H., Galloway, D. K., & Price, D. J. 2013, ApJ, 772, 94
Yakovlev, D. G., & Pethick, C. J. 2004, ARA&A, 42, 169
Yuan, F., & Cui, W. 2005, ApJ, 629, 408
Zampieri, L., Turolla, R., Zane, S., & Treves, A. 1995, ApJ, 439, 849
Zavlin, V. E., Pavlov, G. G., & Shibanov, Y. A. 1996, A&A, 315, 141
Zurek, D. R., Knigge, C., Maccarone, T. J., Dieball, A., & Long, K. S. 2009, ApJ, 699, 1113